AALBORG UNIVERSITY
STUDENT REPORT

Master's Thesis

Analysis of Bolted Joints in Steel Structures

Aalborg University
March 2024
Hariesh Arulanantham

AALBORG UNIVERSITY
STUDENT REPORT

Department of the Built Environment
Structural and Civil Engineering
Thomas Manns Vej 23
9220 Aalborg Øst
www.build.aau.dk

Title:

Analysis of Bolted Joints in Steel Structures

Project period:

April 2023 - March 2024

Written by:

Hariesh Arulanantham

Supervisors:

Lars Pedersen
Christian Frier

Pages: 101
Submission date: 01.03.24

Synopsis:

In this thesis different methods of modelling a bolted end-plate steel joint are considered and how different joint configurations influences a frame. The investigated frame is a portal frame with fixed supports.
The non-linear behaviour of several joint configurations are predicted using two methods of analysis and are compared. The first method investigated is the Component Method, which is the method used in Eurocode 3 and the second is the numerical method where simulations are carried out in the commercial software ANSYS.
Using the obtained moment-rotation curves, the influence of the joint, in regards to the global structure, is investigated. Two methods of analysis are used, the first is the Slope-deflection method, which is an analytical method, and the second being the numerical method where the commercial software RFEM is used.
In conclusion the numerical determined joint behaviour with bolts close to the edge of a thin end-plate shows a lesser bending moment resistance compared to the analytical method. The numerical model shows a greater bending moment resistance for the rest of the configurations. The frames moment distribution shows a correlation between the two methods. The difference are due to the Slope-Deflection method is a linear-elastic method.

Readers guide

Where sources have been used, references to the source are given with the author(s) surname(s) and the year of publication. If the source is used actively in the associated content, the reference is presented as surname(s), year of publication. If the source is used passively, the reference is presented as [surname(s), year of publication]. Figures, tables and expressions are consecutively numbered with respect to the chapter in which they are presented, which means that e.g. third figure of chapter six is named figure 6.3. The specification of the name and number will appear just below figures and tables, whereas the numbering of expressions will appear close to the right-margin of the page. Figures without references are composed by the author of the report.

Referat

I dette speciale vil den ikke-linære adfærd for en boltet tværplade samling blive undersøgt for en satellitramme eller portalframe, som det kaldes på engelsk. Rammens understøtninger er indspændte. Der vil blive opstillet forskellige konfigurationer af samlingen, hvor der vil undersøges, hvad der har indflydelse på samlingens arbejdskurve og moment bæreevne. To metoder vil blive undersøgt og sammenlignet. Den første er Komponent Metoden, der er en analytisk metode som benyttes i Eurocode 3. Den anden metode er den numeriske metode, hvor finite element programmet ANSYS benyttes.

Når den ikke-linære arbejdskurve er bestemt, vil den blive brugt til at undersøge den indflydelse en samling har på rammekonstruktionen. Rammens momentfordeling vil undersøges ved brug af to metoder. Den første metode er Slope-Deflection metoden, som er en analytisk metode, samt finite element programmet RFEM. De to metoder vil blive sammenlignet ved brug af de ikke-linære arbejdskurver, der er blevet bestemt.

Moment bæreevnen bestemt med den analytiske metode og den numeriske metode viser en afvigelse. Moment bæreevnen er mindre ved den numeriske metode for boltplaceringer, der er placeret tæt ved en tynd tværplades kant. Det omvendte er gældende ved de samlings konfigurationer, hvor bolt-placeringen er tættere mod midten af tværpladen. Her giver den numeriske metode en større moment bæreevne.

Sammenligningen mellem momentfordelingerne bestemt analytisk og numerisk viser en afvigelse. Dette skyldes, at den analytiske model antager at materialemodellen er linærelastisk, hvorimod at den numeriske model benytter en materialemodel, der ikke er linær.

Contents

Introduction

1. Introduction

An introduction to the study will be presented in this chapter as well as the motivation and thesis outline for this paper.

1.1 Background

The first use of steel as a structural material dates back to the mid-19th century and is now one of the most used structural materials. It is used in structures as skyscrapers, wind turbines and bridges and can be used alongside concrete, also known as a composite structure. Many known structures are made of steel, one of which is the Golden Gate Bridge as seen in figure 1.1. [Vayas et al., 2019]

Figure 1.1: Picture of the Golden Gate Bridge which is a steel structure. [Unsplash, 2018]

The traditional steel construction consist of an assembly of beams and columns, which assembled results in a combination of steel frames. The connections between the different elements plays a crucial role in the design of structural frames. They are responsible for transferring forces between structural elements and ensuring the overall stability and integrity of the structure. Thus predicting the behaviour of the connections is essential to achieve a safe structure and simultaneously offer a solution which is economical sound and cost-effective. The

design of connections and joints are mandated by national standards while Eurocode specifies how structural design should be conducted within the European Union.

Eurocode 3 applies to the design of steel buildings and is concerned with the requirements for the resistance, serviceability, durability and fire resistance [Dansk Standard, 2022]. Part 1-8 of Eurocode 3 provides methods to design mechanical and welded joints subjected to mostly static loads in steel grades S235, S275, S355 and S460 [Dansk Standard, 2007]. The standard takes the various factors that can affect the performance of these connections into account, such as the material properties of the steel, the load conditions, and the environmental factors.

Joints can be distinguished as either a mechanical connection or as a welded connection. The two types of connections are assembled differently and the preferred joint depends on a variety of factors, including the necessary strength, durability, flexibility and method of installation. Figure 1.2 illustrates the two types of joints. [Vayas et al., 2019]

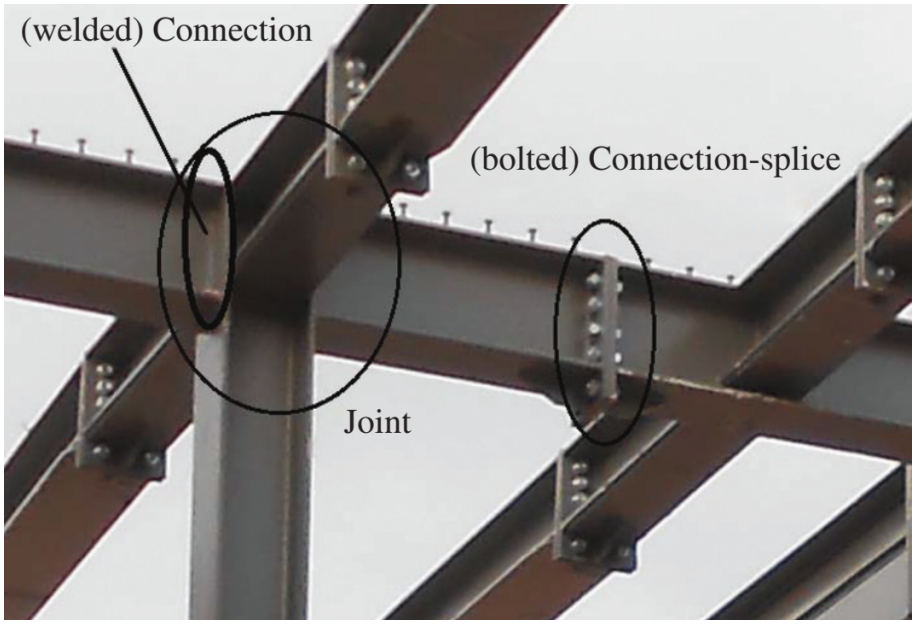

Figure 1.2: Example of a welded and bolted connection [Vayas et al., 2019].

Connections and joints are distinguished as two different things. A connection is the location where two or more structural elements meet, whereas a joint refers to the zone where multiple members are interconnected. For design purposes the connection is all the basic components which connects the structural elements while the joint is all the basic components required to depict the behaviour during the transfer of internal forces and moments. Figure 1.3 shows the definition of a connection and a joint for a beam-to-column joint configuration. **1** is the web panel in shear, **2** is the connection and **3** is the components e.g. the bolts and end-plate. [Dansk Standard, 2007]

A welded connection would attract a different load compared to a bolted connection under the same circumstances, due to different stiffness. Welded connections tend to be stiffer than bolted connections, and would therefore attract a larger portion of the applied load. [Vayas et al., 2019]

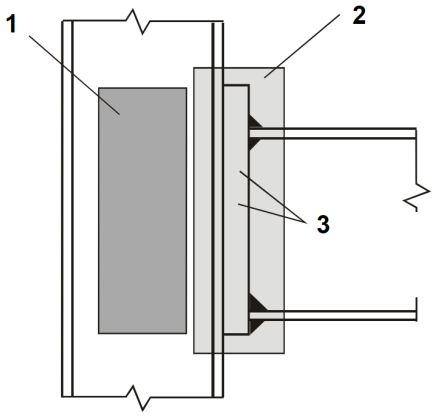

Figure 1.3: Part of a beam-to-column joint configuration, where **1** is the web panel in shear **2** indicates a connection and **3** illustrates the components e.g. the bolts and end-plate. [Dansk Standard, 2007].

This thesis will investigate bolted beam-to-column steel joints with an end-plate connection. The beam and end-plate are welded together such a bolted connection can be established between the end-plate and the column flange. The welded part of the joint will not be investigated.

1.2 Motivation behind the study

A mechanical connection is a connection which joins two or more structural elements together with bolts, rivets, pins etc. The Golden Gate Bridge, see figure 1.1, are held together with rivets and bolts [Golden Gate Bridge, Highway and Transportation District, 2024]. In the present time, bolt assemblies are the most used fastener to connect plates or profiles. A bolt assembly consist of the bolt itself, a nut and one or more washers, see figure 1.4. All parts of a bolted joint, needs to comply with the standards listed in section 1.2.4 of Eurocode 3 Part 1-8. [Jaspart and Weynand, 2016]

Figure 1.4: Example of bolt assemblies [Jaspart and Weynand, 2016].

Modelling a steel joint has its benefits, although an experimental analysis can provide the necessary result, it can be costly to test a full-scale joint [Augusto et al., 2015]. Establishing a numerical model and simulating the behaviour of the joint, can therefore be cost-effective, given the developed finite element models depicts the real behaviour of the real joints. There are five different methods for predicting joint behaviour and can be divided into: numerical models, mechanical models, physicals models, empirical models and analytical models [Faella et al., 1999].

Mechanical modelling of a joint has gained vast recognition due to the balance between accuracy and its simplicity. Eurocode 3 establishes a method of modelling a joint using the mechanical method. Numerical modelling does provide a more realistic representation of the joint behaviour compared to the mechanical model, but is more time consuming. [Augusto et al., 2015]

The findings of a numerical model can although not be blindly trusted. An error can lead to results which can deviate substantially from the real behaviour and therefore different methods of obtaining the desired results should be conducted and compared. The numerical model should also be realistic such as depicting the real behaviour of the bolts, contact pressure between the individual components etc.

1.3 Thesis outline

This thesis will examine a portal frame with fixed supports and determine the moment bearing capacity of the beam-to-column joint with four different joint configurations. Two of the joint configurations have a bolt placement close to the centre of the end-plate and the other two are close to the edge of the end-plate. The bending moment distribution of the portal frame will also be investigated and obtained for different beam-to-column joint stiffness's. The first part of this thesis will study the behaviour of the joint while the second part will examine the whole global structure.

A vertical distributed load is applied on the beam of the frame. The load is assumed constant over the entire beam and the column supports are assumed fixed with no rotational movement and translational motion, see figure 1.5.

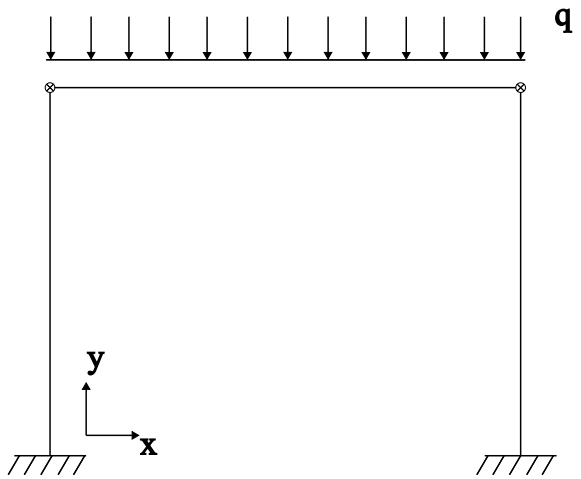

Figure 1.5: The portal frame with fixed supports, and a vertical distributed constant load q.

This thesis will not consider the design of the portal frame and therefore only the characteristic values will be used. The cross-section used for the beam and columns are traditionally used profiles and the geometrical properties are taken from Jensen et al., 2022.

1.3.1 Moment bearing capacity

The following models are used to determine the moment bearing capacity of the beam-to-column joint and the moment distribution of the frame.

- Mechanical model
- Finite element model

The design code of joints in Eurocode 3 Part 1-8 is based on the Component Method, which is a mechanical model that can be used to determine the moment bearing capacity of a joint. This method is based upon the rotational response of the joint being dependent on the mechanical properties of the individual components of the joint. So the joint configuration is decomposed into its basic components. Each basic component can be represented by a linear or non-linear spring, which describes the properties of the component. This method of obtaining the joints stiffness and moment bearing capacity will be further studied in this thesis. [Weynand et al., 1995]

The finite element model has the advantage of not being limited by the geometry and therefore easier to build and analyse the joints. The finite element program ANSYS will be used to determine the moment bearing resistance.

Four different joint configurations are investigated, to analyse the effect the bolt-placement has in regards to the distance to the end-plate edges. Three different end-plate thickness are also investigated and implemented in the four joint configurations.

1.3.2 Bending moment distribution

To determine the bending moment distribution of the frame the following models will be used:

- Analytical model
- Finite element model

The analytical model used is derived from the "slope deflection method", which is a structural analytical method for beams and frames. The method is used to determine the end-moments of the columns and beams.

The finite element software used is RFEM, and it is a commercial program. The results are compared to the moment distribution determined from the analytical model.

1.4 Problem definition

The following objectives are made, so that the described thesis outline can be solved.

- Understand the requirement to determine the joint bearing capacity according to Eurocode 3
- Understand the underlying theory of the Component Method
- Determine the moment bearing capacity of steel joints using the Component Method
- Perform a numerical analysis of a joint and compare the moment bearing resistance to the model of Eurocode 3
- Determine the moment distribution of the frame using an analytical model
- Determine the moment distribution of the frame using RFEM and compare the results with the analytical method
- Use the moment-rotation curve to determine the bending moment at the joint under a loading condition of the frame

2. Initial considerations

In this part the portal frame and the joints is described and is illustrated in figure 2.1 and figure 2.2. The dimensions of the column, beam, end-plate and bolts are presented and are presented in table 2.2. The column, beam, bolts and end-plate are all kept constant except for the end-plate thickness.

2.1 Joint configurations

The joint consist of different parts. The parts are listed as followed:

- Column
- Beam
- End-plate
- Bolts

The material for all parts are of steel. The end-plate is welded to the beam and the end-plate is connected to the column with the bolts. The bolts consists of a header, washer, shaft, thread and nut. The head and nut of the bolt are then able to interlock the end-plate and column together. The static system which is being analysed is illustrated in figure 2.1 (a). The supports of the frame are fixed. The frame is subjected to a vertical linear distributed load q. The columns and beam of the frame is connected as illustrated in figure 2.1 (b) and the connection consists of two bolt-rows. The beam and end-plate are welded together. The weld is assumed stronger than the rest of the joint and is also assumed that it does not deform under a loading condition.

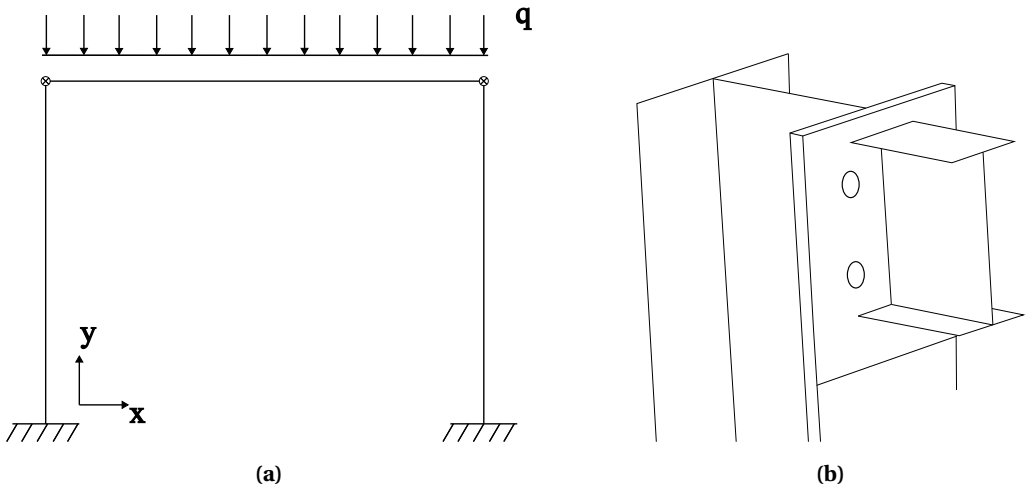

Figure 2.1: Illustrations of (a) the considered frame (b) the considered joint.

The analysis of the joints moment bearing capacity consists of four different joint configurations. The beam and column are kept the same for all configurations, whereas the bolt-placement and end-plate thickness varies. The bolt-placement and beam-placement are shown in figure 2.2. The edge distances e_1 and e_2 varies while the distance between the bolt-rows p_1 are kept constant

at 100 mm. e_1 and e_2 are in compliance with Eurocode 3 Part 1-8 as the minimum edge distance is $1,2d_0$, where d_0 is the hole diameter for the bolt, see table 2.2.

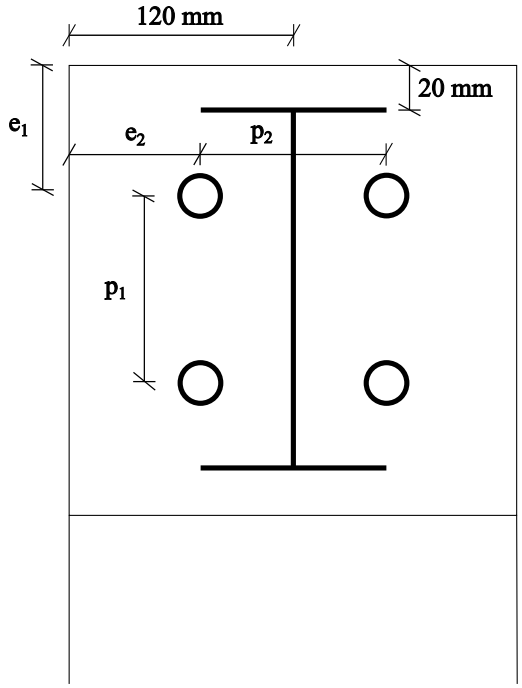

Figure 2.2: The placements of the beam and bolts.

The four joint configurations are named Model 1-4 and described in table 2.1. The motivation is to analyse the effect the bolt placement has in regards to the distance to the end-plate edge.

	e_1 [mm]	e_2 [mm]	p_1 [mm]	p_2 [mm]
Model 1	70	70	100	100
Model 2	35	35	100	170
Model 3	45	70	100	100
Model 4	70	45	100	150

Table 2.1: Description of the joint configuration.

The dimensions and material properties of the beam, column, bolts and end-plate are shown in table 2.2. For all the joint configurations the moment bearing capacity are determined for a end-plate thickness of 10 mm, 14 mm and 17 mm.

	Parameter	**Unit**	**Value**
Beam IPE200	Height, h_b	mm	200
	Width, b_b	mm	100
	Thickness of the flange, t_{fb}	mm	8,5
	Thickness of the web, t_{wb}	mm	5,6
	Radius of root fillet, r_b	mm	12
	Moment of inertia, I_y	mm^4	$19,4\,10^6$
	Length of frame, L	mm	5500
Column HE240B	Height, h_c	mm	240
	Width, b_c	mm	220
	Thickness of the flange, t_{fc}	mm	17
	Thickness of the web, t_{wc}	mm	10
	Radius of root fillet, r_c	mm	18
	Moment of inertia, I_y	mm^4	$80,9\,10^6$
	Height of frame, H	mm	3000
End-plate	Height, h_{ep}	mm	240
	Width, b_{ep}	mm	240
	Thickness, t_{ep}	mm	10,14,17
	Hole diameter, d_0	mm	15
Bolt M16	Diameter of shaft, d_i	mm	13,5
	Bolt-head height, h_b	mm	10
	Nut height, h_{nut}	mm	13
	Washer diameter, d_w	mm	30
	Washer thickness, t_w	mm	3
Steel	Yield strength, f_y	MPa	235
	Yield strength bolts, f_{yb}	MPa	640
	Modulus of elasticity, E	MPa	$2,1\,10^5$
	Poisson's ratio, ν		0,30

Table 2.2: The parameters and the value used for analysing the steel frame [Jensen et al., 2022].

The dimensions of the beam an columns are shown in figure 2.3 (a) as well as the axis for the moment of inertia. The dimensions of the bolts are shown in figure 2.3 (b).

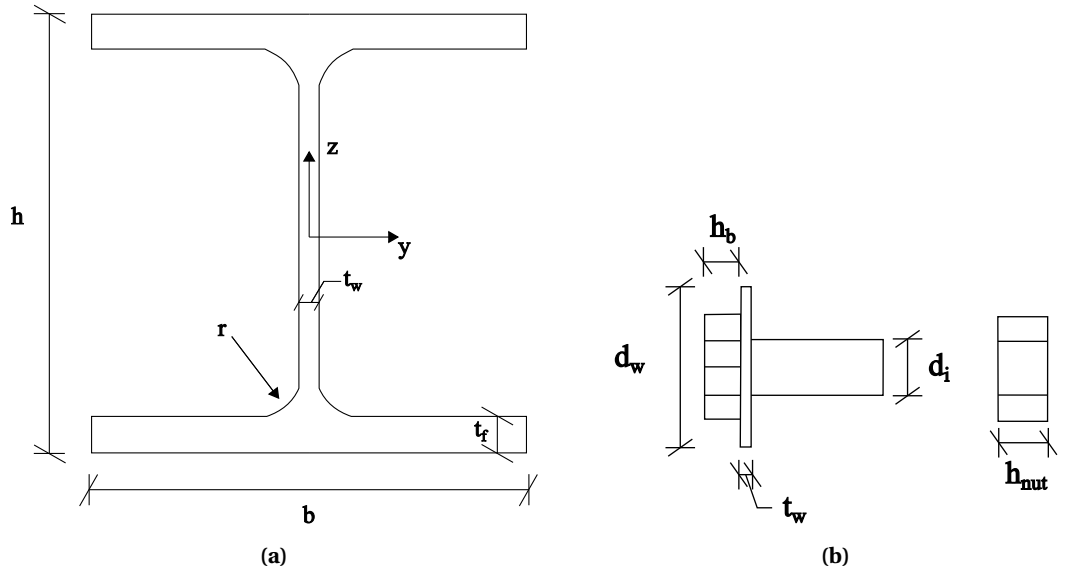

Figure 2.3: Dimensions of (a) the beam and columns (b) the bolts.

2.2 Material behaviour

The material used is steel. Eurocode 3 Part 1-1 provides the characteristics values for the chosen steel grade of the column, beam and end-plate. The chosen steel grade is S235 and the given characteristics values of yield strength and ultimate tensile strength are shown in table 2.3. The nominal properties for the bolts are dictated by Eurocode 3 Part 1-8. The characteristic strength properties of the bolts are given in table 2.3.

	Elements [MPa]	Bolts [MPa]
Yield strength	235	640
Ultimate tensile strength	360	800

Table 2.3: characteristics strength values for the elements (beams and columns) and bolts.

The internal forces and moments can either be determined by an elastic or plastic global analysis. An elastic global analysis can be used in all cases and is based on the assumption the stress-strain relation of a material is linear. For the plastic global analysis only steel grades up to S460 and if the the cross-sections of the beam and column are classified as a class 1 can be analysed. The method of global analysis is elastic-perfectly plastic. The stress-strain relation for steel as a elastic-plastic material is shown in figure 2.4 [Dansk Standard, 2022].

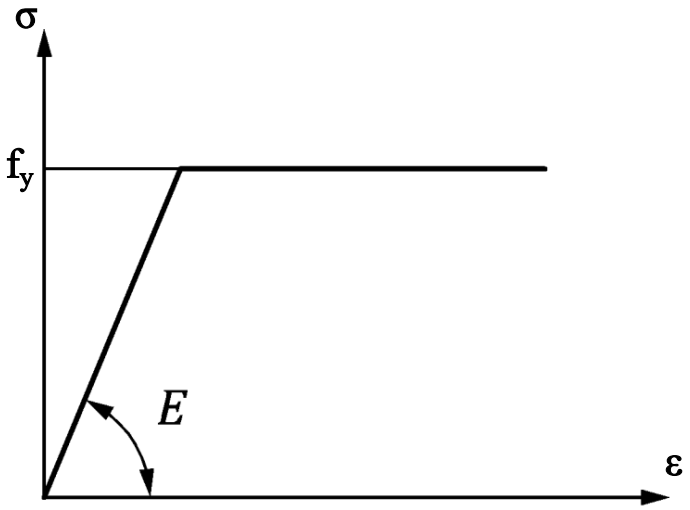

Figure 2.4: The stress-strain relation for steel.

II Moment bearing capacity

3. Structural properties

In this chapter the structural properties of a joint is presented. The moment-rotation curve is described for joints in general.

The members of a joint, can be represented by its centre-lines which is connected by a rotational spring. Figure 3.1(a) illustrates a single-sided beam-to-column joint configuration whereas figure 3.1(b) illustrates the centre lines being connected. [Dansk Standard, 2007]

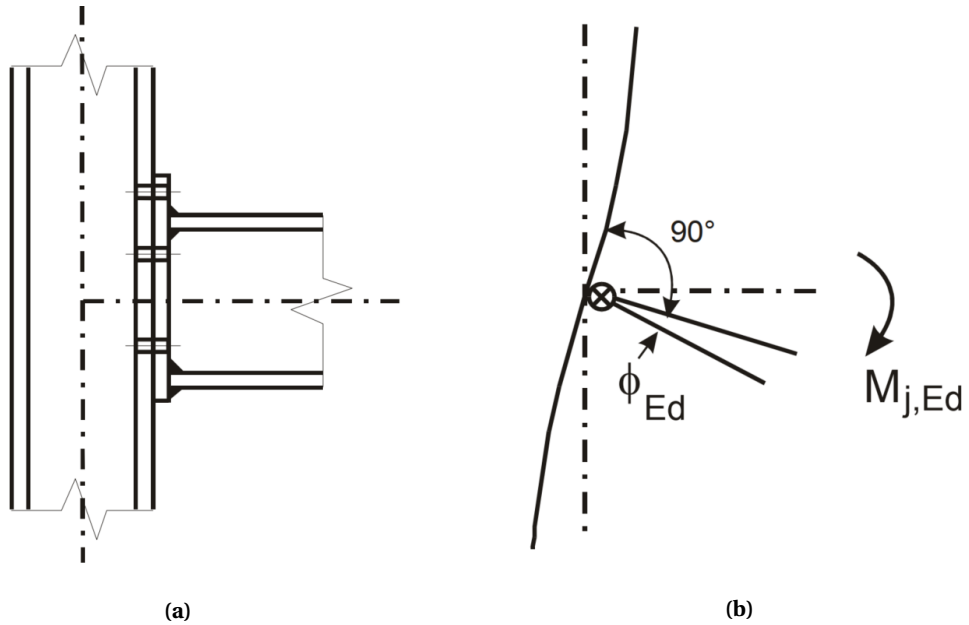

(a) **(b)**

Figure 3.1: Illustration of; (a) single-sided beam-to-column joint configuration, (b) the centre lines of the joint configuration [Dansk Standard, 2007]

The rotational spring can be expressed with the relationship between the bending moment $M_{j,Ed}$ and the corresponding relative rotation Φ_{Ed} between the connecting members. This relation is also called the design moment-rotation relation and should describe the following three characteristics of the joint [Dansk Standard, 2007]:

- Moment resistance $M_{j,Rd}$
- Rotational stiffness S_j
- Rotational capacity Φ_{Cd}

The design moment-rotation characteristics can be derived from the $M-\Phi$ curve, see figure 3.2. The curve consists of three parts; a linear part, a non-linear part and a yield plateau. The first part of the curve is linear with the corresponding stiffness called the initial stiffness $S_{j,ini}$, which resembles the slope. The linear part is assumed to end at $2/3M_{j,Rd}$ where the non-linear part begins, as it is assumed that yielding of the material occurs. The stiffness at the non-linear part is described as the secant stiffness S_j. The yield plateau is reached when $M_{j,Ed}$ is equal to $M_{j,Rd}$, and the stiffness can no longer be described. [Weynand et al., 1995]

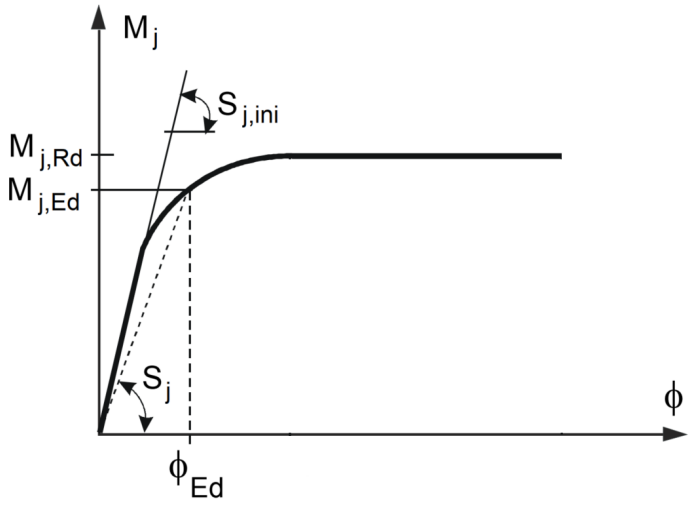

Figure 3.2: The design moment-rotation characteristics [Dansk Standard, 2007].

The design moment-rotation characteristics of a joint is required to properly model joints behaviour. Several methods can be used to model the design moment-rotation characteristics where the Component Method and the numerical method is used.

4. Component Method

The purpose of this chapter is to introduce the Component Method from Eurocode 3 Part 1-8 which is the mechanical model. The general model of the Component Method is described in appendix A. The calculations are presented to determine the joint stiffness and moment bearing capacity. The bolt placement are showed in figure 2.2 and table 2.1. A worked example of Model 1 with end-plate thickness of 10 mm are shown in appendix B.

The Component Method is a method of determining the design moment-rotation characteristics of a joint by decomposing it into a set of individual components. Each of the components are modelled as non-linear springs, each having individual stiffness's and resistances. Figure 4.1 illustrates the spring model for a beam-to-column end-plated joint with two bolt-rows in tension. The springs k_1 and k_2 represents the components in shear and compression. The springs $k_{3,r}$, $k_{4,r}$, $k_{5,r}$ and $k_{10,r}$ represents the components in tension for bolt-row r. This is also the spring model for Model 1-4. [Weynand et al., 1995]

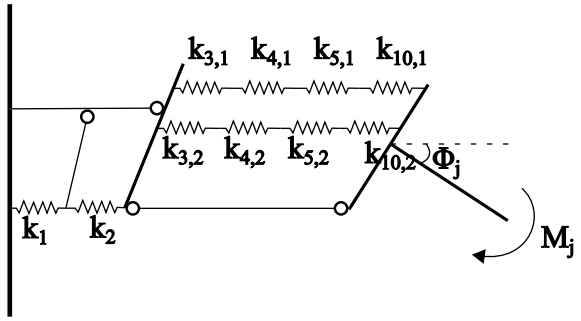

Figure 4.1: The spring model for a one-sided beam-to-column end-plated joint with two bolt-rows in tension [Weynand et al., 1995]. This is also the spring model for Model 1-4.

The stiffness coefficients of the individual components are used to determine the overall rotational stiffness. This is done with the procedure given in Eurocode 3 Part 1-8. For a single-sided bolted end-plate beam-to-column joint with two or more bolt-rows in tension, the stiffness coefficients to be taken into account are; k_1, k_2, k_3, k_4, k_5 and k_{10}. The stiffness coefficients are obtained from the following basic components:

- k_1 - Column web panel in shear
- k_2 - Column web in compression
- k_3 - Column web in tension
- k_4 - Column flange in bending
- k_5 - End-plate in bending
- k_{10} - Bolts in tension

The design procedure according to Eurocode 3 Part 1-8 can be divided into three steps. The steps are the following:

- Identify the relevant components
- Characterise the individual components strength and stiffness properties

- Assemble the individual components and determine the joints structural properties

For an end-plate column-to-beam connection mainly subjected to bending the relevant components can be divided in three different zones; *compression, shear and tension.* Figure 4.2 illustrates a bolted end-plated joint where the bending moment is split into a tension and compression force. [P., 2000]

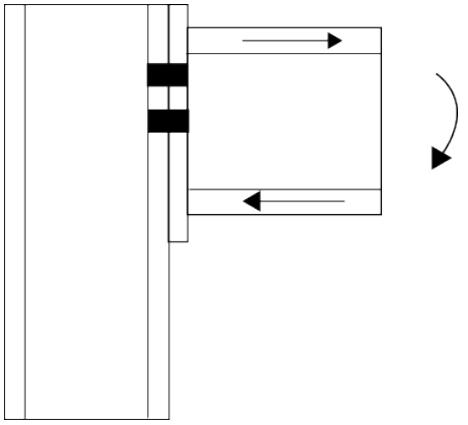

Figure 4.2: The bending moment resulting in a tension and compression zone.

The basic components can then be divided into each of the zones which all has its own strength and stiffness. The three zones are as follows with the relevant components:

- Compression zone:
  - Beam flange and web in compression
  - Column web in compression
- Shear zone
  - Column web panel in shear
- tension zone
  - Column web in tension
  - Column flange in bending
  - Bolts in tension
  - End-plate in bending
  - Beam web in tension

According to Eurocode 3 Part 1-8 the design moment bearing $M_{j,Rd}$ is determined by equation (4.1).

$$M_{j,Rd} = \sum h_r F_{tr,Rd} \tag{4.1}$$

Where

h_r	is the distance from bolt-row r to the centre of compression, see figure4.3
$F_{tr,Rd}$	is the effective design tension resistance of bolt-row r

The effective design resistance $F_{tr,Rd}$ for bolt-row r is taken as the smallest design tension resistance of the basic components in tension. The number of bolt-rows are defined from the

joint configuration. Figure 4.2 has two bolt-rows, where the bolt-row furthest from the centre of compression, is the first bolt-row while the second bolt-row is the closest to the centre of compression. This is illustrated in figure 4.3.

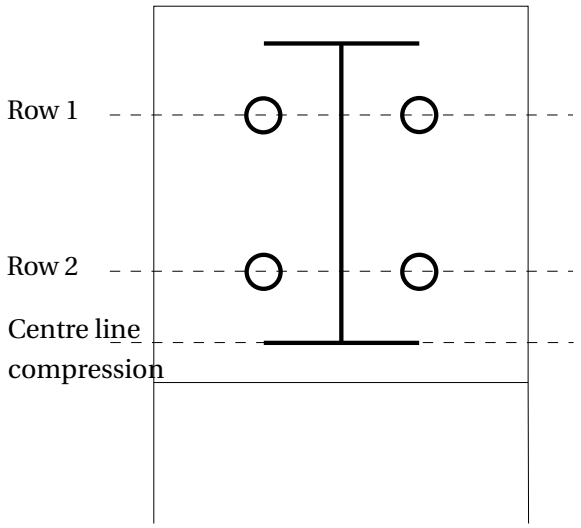

Figure 4.3: Illustration of bolt-rows numbering and centre line of compression

The bearing resistance of the components in shear and compression are then checked against the tension resistance. If the tension resistance is greater than the shear or compression resistance, it is then reduced. The moment bearing resistance is determined from the components which are in tension. The components in tension, compression and shear are listed earlier. The equivalent T-stub methodology is used to model the components in tension and determine the design tension resistance which then can be used to obtain the moment bearing capacity with equation (4.1). [Dansk Standard, 2007]

4.1 Equivalent T-stub

The equivalent T-stub method is an geometric idealisation of plates subjected to transverse forces. The name comes from the appearance of the geometry and consists of a web in tension and a flange i bending, see figure 4.4. The T-stub has the advantage that a component in bending and tension can be studied with the model.

The visualisation of a T-stub in a bolted joint with the end-plate and the column flange is shown in figure 4.5. The figure also shows that the T-stub approach should be done to both sides of a joint as both the end-plate and column flange can be represented as a T-stub.

When the T-tub is subjected to a tension force, the flanges of the T-stub deforms due to bending and the bolts elongate due to the tension forces. Failure occurs when either yield lines around the bolt develops or the bolts being in failure. [Zoetemeijer, 1974]

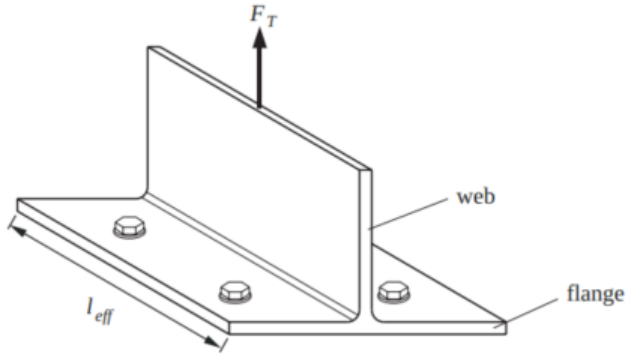

Figure 4.4: Geometry of a bolted T-stub [Jaspart and Weynand, 2016].

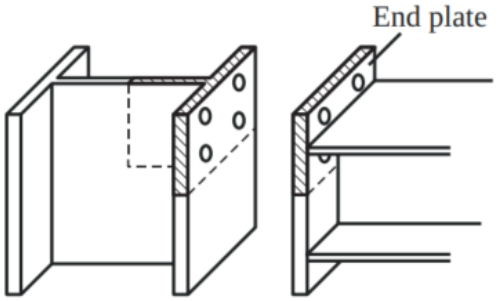

Figure 4.5: Visualisation of a T-stub of a bolted joint [Jaspart and Weynand, 2016].

4.1.1 Failure modes of the T-stub

The failure modes of a T-stub is based on the plastic behaviour of the flanges and bolts, where plastic hinges are eventually formed at the bolts and/or the flanges. The failure of a T-stub is either due to failure of the bolt, plastification of the flange plate or a combination of the two. [Zoetemeijer, 1974]

The resistance of the T-stub can be determined from three possible failure modes. The three failure modes are given as:

- Failure mode 1 - yielding of the flange
- Failure mode 2 - failure of bolts and partial yielding of the flange
- Failure mode 3 - failure of bolts

Failure mode 1 occurs when the flanges are yielding and is associated to the formation of plastic hinges in the flange and development of the prying force Q, see figure 4.6(a). Prying forces are forces which develops due to the contact between the beam and column flange. It is further explained in chapter 4.1.2. The bolts are sufficiently strong enough to resist the the applied tension force and the prying forces which leads to the flanges yielding before the bolts tension resistance is reached.
Failure mode 2 occurs when tensile failure of the bolts and partial yielding of the flange happens at the same time. Yield lines in the flanges develops, but not to the same extent as the full plastic mechanism in failure mode 1, see figure 4.6(b). Prying forces also develops in this failure mode.

Failure mode 3 is the failure of bolts. No prying forces develops as the flange does not yield, so there only occurs failure of the bolts, see figure 4.6(c).

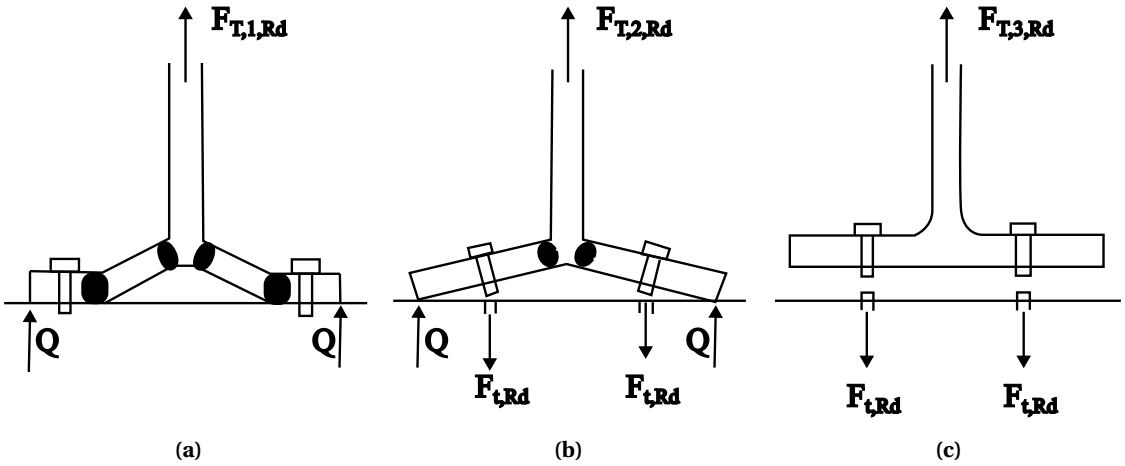

Figure 4.6: The failure modes of an equivalent T-stub where (a) is failure mode 1 (b) is failure mode 2 and (c) is failure mode 3.

The three different failure modes results in different design resistance and is determined for each bolt-row as well as the bolt-row groups. The failure mode which results in the lowest bearing capacity is the design bearing resistance for the considered bolt-row or bolt-row group.

4.1.2 Prying force

Prying forces will develop if the bolt can not elongate significantly when the T-stub is under tension. This will result in a clamping effect between the flanges in contact. Figure 4.6(a) shows the prying force Q on a T-stub in tension. The sum of the transferred forces will increase, if prying forces develops, this is also illustrated in figure 4.6(a). If the bolt can elongate enough, the prying forces will have a negligible effect and can therefore be disregarded. To determine whether the bolt has a significant elongation, EC3 Part 1-8 provides a criterion, which if satisfied can be concluded that prying forces will develop, see equation (4.2). [Jaspart and Weynand, 2016]

$$L_b \leq \frac{8,8m^3 A_s n_b}{\sum l_{eff,1} t^3} \tag{4.2}$$

Where:

L_b	is the elongation length, taken as the total thickness of material and washer, plus half the sum of the height of the bolt and height of the nut
t	is the thickness of the T-stub flange
m	is a geometrical length which represent the distance between the bolt axis and the point where the "potential" plastic hinge will form, see figure 4.15
n_b	is the number of bolts in one bolt-row
l_{eff}	is the effective length and is explained in chapter 4.1.3

If prying forces develop equation (4.15) and equation (4.16) are used to determine the bearing resistance for failure mode 1. Equation (4.17) is used to determine the bearing resistance for failure mode 2. Otherwise equation (4.18) is used for both failure modes.

4.1.3 Effective length

The effective length l_{eff} is a theoretical length and is defined as the equivalence between the actual component and the T-stub idealisation in the plastic stage where yield line develops. The possible yield lines characterise the effective length. Eurocode 3 Part 1-8 presents two different failure patterns with yield lines and expressions of l_{eff} according to the failure patterns. The failure patterns are only according to failure mode 1 and 2 as failure mode 3 does not develop any yield lines at the flange. Figure 4.7 shows the different failure patterns and that the failure patterns can be described as either **circular** or **non-circular**. [Jaspart and Weynand, 2016]

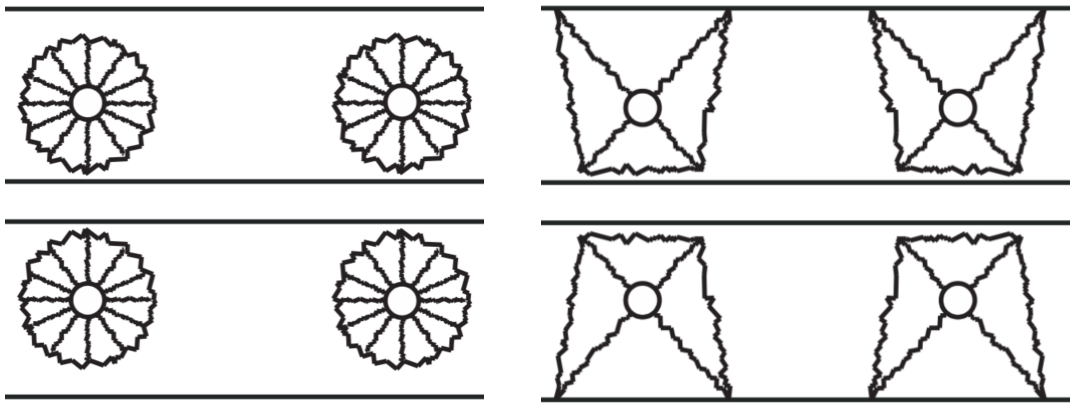

(a) **(b)**

Figure 4.7: Illustrations of (a) circular yield patterns (b) non-circular yield patterns [Jaspart and Weynand, 2016].

As seen on figure 4.7 two types of yield line patterns can develop. Each of the yield lines can develop when considering bolt-rows individually and bolt-rows as part of a group of bolt-rows. Figure 4.8 illustrates the yield line patterns for a group of bolt-rows. Figure 4.8(a) illustrates the yield lines for a circular failure pattern and figure 4.8(b) illustrates the yield lines for a non-circular pattern. [Dlubal, 2023a]

The failure patterns characterises the effective length. Zoetemeijer, 1974 establishes a method to determine the effective lengths using plasticity theory and assuming that the elastic deformations are negligible. For failure mode 1 the collapse of the flange is seen in figure 4.9 for a non-circular pattern. The failure patterns are observed through experiments and expressions of the effective lengths are then determined. B_t is the bolt force, T is the tensile load and $\Delta\delta$ is the plastic deformation. B_t and T are equal if no prying forces develop. The unknowns which are solved for are α and β. The angles are solved so it produces the smallest tension load.

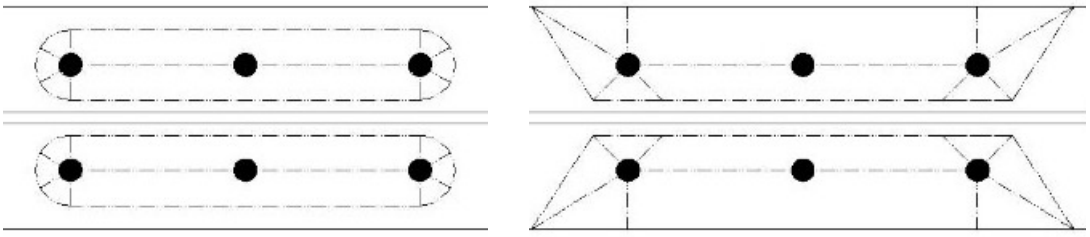

(a) **(b)**

Figure 4.8: A bolt of groups with (a) circular yield lines (b) non-circular yield lines [Dlubal, 2023a].

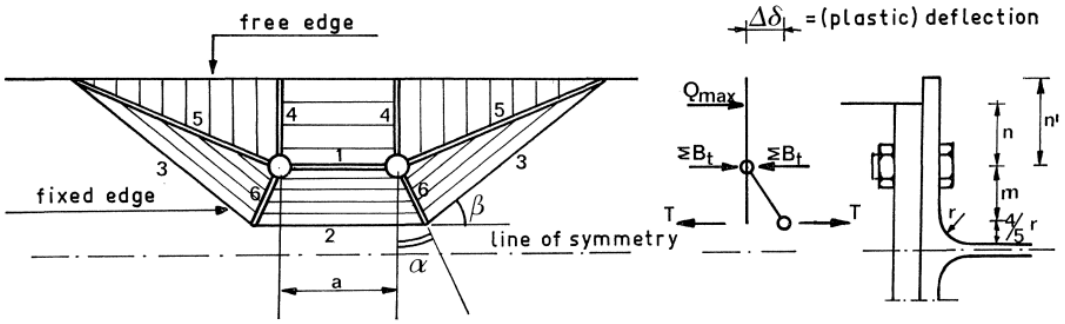

Figure 4.9: Collapse of flange for failure mode 1 [Zoetemeijer, 1974].

The internal dissipation energy, ΔE is set equal to the work done by the external force ΔT, see equation (4.3). When the yield lines develop at the bolts, the bolt force does not affect the external force as no displacement occurs at the bolts, see figure 4.9.

$$\Delta E = \Delta T \tag{4.3}$$

The work done by the external forces is given in equation (4.4).

$$\Delta T = T\Delta\delta \tag{4.4}$$

Expressions for the six yield lines given in figure 4.9. The internal dissipation energy and rotation are determined through geometric relations and given in equation (4.5) to equation (4.10). [Zoetemeijer, 1974]

$$\Delta E_1 = a\frac{\Delta\delta}{m}m_p \tag{4.5}$$

$$\Delta E_2 = (a+2m\tan\alpha)\frac{\Delta\delta}{m}m_p \tag{4.6}$$

$$\Delta E_3 = 2\frac{m+n'}{\sin\beta}\frac{\cos\alpha}{\cos(\beta-\alpha)}\frac{\Delta\delta}{m}m_p \tag{4.7}$$

$$\Delta E_4 = \frac{2n'}{b}\Delta\delta m_p \tag{4.8}$$

$$\Delta E_5 = 2\left(\cot\beta + \frac{n'}{m}\frac{\cos\alpha}{\sin\beta\cos(\beta-\alpha)} - \frac{n'}{b}\right)\Delta\delta m_p \tag{4.9}$$

$$\Delta E_6 = \frac{2m}{\cos\alpha}\frac{\Delta\delta}{m}\frac{\sin\beta}{\cos(\beta-\alpha)}m_p \tag{4.10}$$

Where:

m_p	is the yield moment per unit length of the plate
n'	is the distance from the centre-line of the bolt to edge of the flange, see figure 4.9
n	is the distance from the centre-line of the bolt to the edge of the plate, see figure 4.9
m	is the distance from centre-line from the bolt to yield line closest to the web
a	is the distance between the bolts
b	is the free edge distance from yield line 4 to yield line 5

The bolts are assumed to only be influenced by elastic deformations. The total internal energy is then set equal to the work done by the external force, see equation (4.3). This can be reduced to equation (4.11).

$$T\Delta\delta = 2\left(\frac{a}{m} + \frac{m+2n'}{m} - \frac{\cos\alpha}{\sin\beta\cos(\beta-\alpha)} + \tan\alpha + \cot\beta + \frac{\sin\beta}{\cos\alpha\cos(\beta-\alpha)}\right)\Delta\delta m_p \tag{4.11}$$

From equation (4.11) it can be observed that minimising the load T will result in minimising the right hand side of the equation. If equation (4.12) is satisfied the minimum value is found using the angles α and β.

$$\frac{\partial\sum\Delta E}{\partial\alpha} = 0, \quad \frac{\partial\sum\Delta E}{\partial\beta} = 0 \tag{4.12}$$

If the partial derivative is carried out and the unknowns α and β are solved the effective lengths can then be determined. The same procedure can be applied to failure mode 2 for a non-circular failure pattern. For a circular pattern the effective lengths are expressed using the circumference of the circular part of the yield lines. The radius is assumed to be m which is illustrated in figure 4.13. For a unstiffened column flange the effective lengths are given in figure 4.10 and for the end-plate components the effective lengths are given in figure 4.11.

Bolt-row Location	Bolt-row considered individually		Bolt-row considered as part of a group of bolt-rows	
	Circular patterns $\ell_{eff,cp}$	Non-circular patterns $\ell_{eff,nc}$	Circular patterns $\ell_{eff,cp}$	Non-circular patterns $\ell_{eff,nc}$
Inner bolt-row	$2\pi m$	$4m + 1{,}25e$	$2p$	p
End bolt-row	The smaller of: $2\pi m$ $\pi m + 2e_1$	The smaller of: $4m + 1{,}25e$ $2m + 0{,}625e + e_1$	The smaller of: $\pi m + p$ $2e_1 + p$	The smaller of: $2m + 0{,}625e + 0{,}5p$ $e_1 + 0{,}5p$
Mode 1:	$\ell_{eff,1} = \ell_{eff,nc}$ but $\ell_{eff,1} \leq \ell_{eff,cp}$		$\sum\ell_{eff,1} = \sum\ell_{eff,nc}$ but $\sum\ell_{eff,1} \leq \sum\ell_{eff,cp}$	
Mode 2:	$\ell_{eff,2} = \ell_{eff,nc}$		$\sum\ell_{eff,2} = \sum\ell_{eff,nc}$	

Figure 4.10: The effective lengths for an unstiffened column [Dansk Standard, 2007].

Bolt-row location	Bolt-row considered individually		Bolt-row considered as part of a group of bolt-rows	
	Circular patterns $\ell_{eff,cp}$	Non-circular patterns $\ell_{eff,nc}$	Circular patterns $\ell_{eff,cp}$	Non-circular patterns $\ell_{eff,nc}$
Bolt-row outside tension flange of beam	Smallest of: $2\pi m_x$ $\pi m_x + w$ $\pi m_x + 2e$	Smallest of: $4m_x + 1{,}25e_x$ $e+2m_x+0{,}625e_x$ $0{,}5b_p$ $0{,}5w+2m_x+0{,}625e_x$	—	—
First bolt-row below tension flange of beam	$2\pi m$	αm	$\pi m + p$	$0{,}5p + \alpha m$ $-(2m + 0{,}625e)$
Other inner bolt-row	$2\pi m$	$4m + 1{,}25\ e$	$2p$	p
Other end bolt-row	$2\pi m$	$4m + 1{,}25\ e$	$\pi m + p$	$2m+0{,}625e+0{,}5p$
Mode 1:	$\ell_{eff,1} = \ell_{eff,nc}$ but $\ell_{eff,1} \leq \ell_{eff,cp}$		$\sum\ell_{eff,1} = \sum\ell_{eff,nc}$ but $\sum\ell_{eff,1} \leq \sum\ell_{eff,cp}$	
Mode 2:	$\ell_{eff,2} = \ell_{eff,nc}$		$\sum\ell_{eff,2} = \sum\ell_{eff,nc}$	

Figure 4.11: The effective lengths for an end-plate [Dansk Standard, 2007].

Considering a joint configuration shown in figure 4.3 both bolt-rows for an unstiffened column flange are considered "end bolt-rows" individually and as part of a group of bolt-rows in figure 4.10. When considering the end-plate, bolt-row 1 is taken as the "first bolt-row below tension flange beam" and bolt-row 2 is taken as "other end bolt-row". To determine the effective lengths for an end-plate, α needs to be established. α is read from figure 4.12. [Dansk Standard, 2007]

To determine α the values of λ_1 and λ_2, which can be determined from equation (4.13) and equation (4.14).

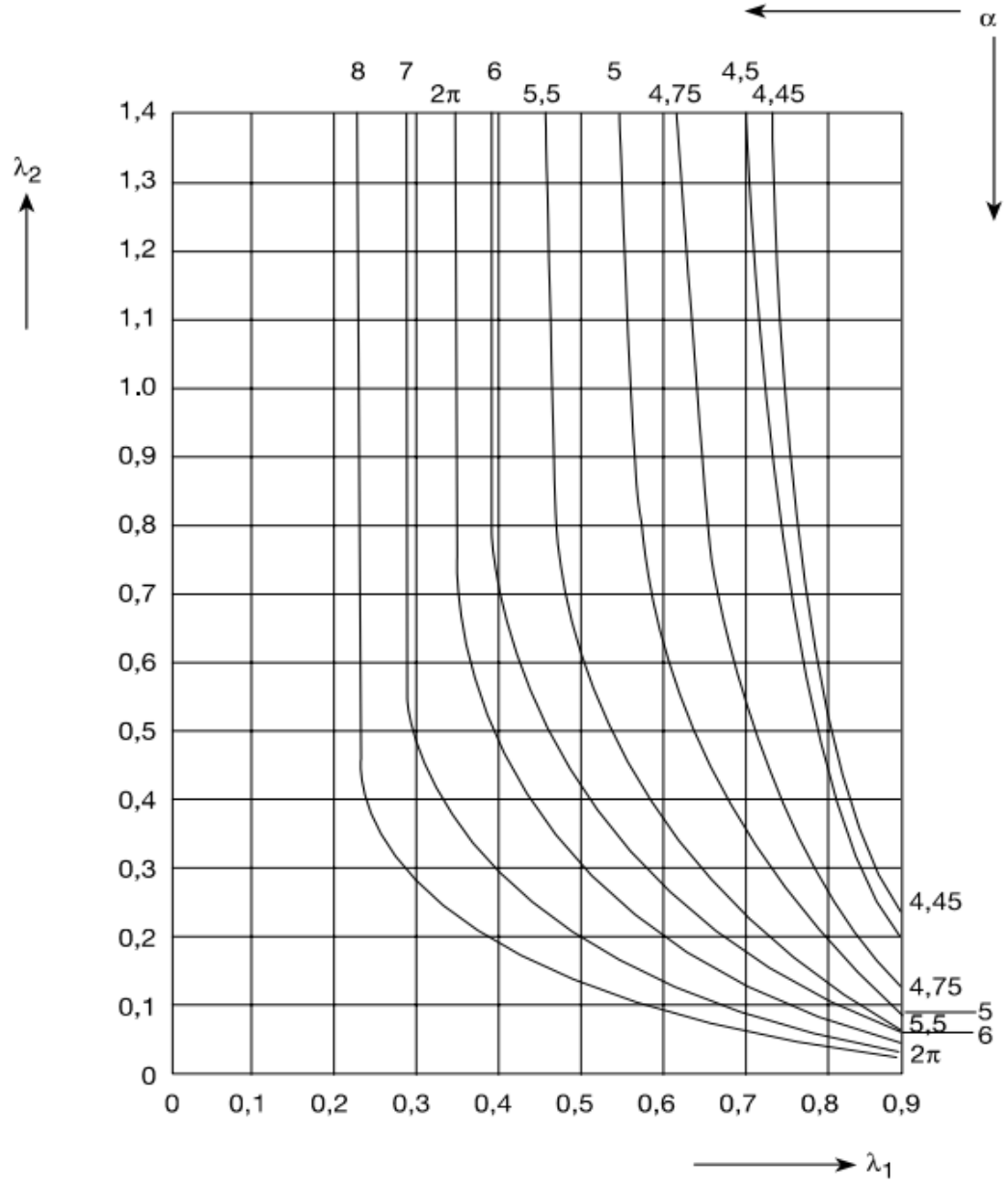

Figure 4.12: Graph of the α-values. [Dansk Standard, 2007].

$$\lambda_1 = \frac{m}{m+e} \tag{4.13}$$

$$\lambda_2 = \frac{m_2}{m+e} \tag{4.14}$$

The parameters m, m_2 and e is defined in figure 4.13. The figure illustrates the end-plate and beam web where the "+" symbols represents the bolts.

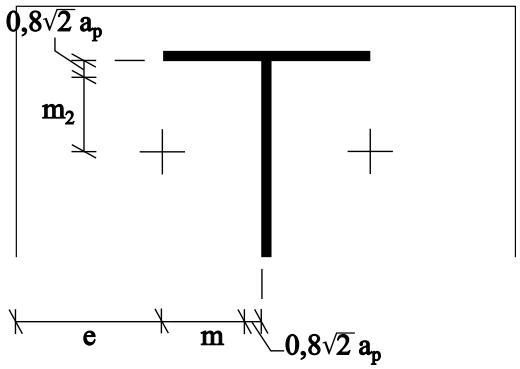

Figure 4.13: Illustration of m, m_2 and e. a_p is the leg size of the weld. [Dansk Standard, 2007].

4.1.4 Design resistance of T-stub in tension

The T-stub consists of a flange and a web, see figure 4.4. The design resistance is determined for the flange and the web individually. As seen in figure 4.5, the column flange and end-plate can be considered the flange on the T-stub. Likewise the column web and beam web can be considered the web of the T-stub. The design resistance of the T-stub flange can be determined according to Eurocode 3 Part 1-8 with the following equations:

Failure mode 1 Yielding of the flange (prying forces may develop):

Method 1:

$$F_{T,Rd,1} = \frac{4M_{pl,1,Rd}}{m} \tag{4.15}$$

Method 2:

$$F_{T,Rd,1} = \frac{(8n-2e_w)4M_{pl,1,Rd}}{2mn-e_w(m+n)} \tag{4.16}$$

Failure mode 2 Partial yielding of the flange and failure of bolts (prying forces may develop):

$$F_{T,Rd,2} = \frac{2M_{pl,2,Rd}+\sum nF_{t,Rd}}{m+n} \tag{4.17}$$

Failure mode 1 and 2 (prying forces does not develop):

$$F_{T,Rd,1-2} = \frac{2M_{pl1,Rd}}{m} \tag{4.18}$$

Failure mode 3 Failure of the bolts

$$F_{T,Rd,3} = \sum F_{t,Rd} \tag{4.19}$$

The design resistance for the T-stub web of the column and beam is given in Eurocode 3 Part 1-8 as equation (4.20) and equation (4.21) respectively.

$$F_{t,wc,Rd} = \frac{\omega b_{eff,t,wc} t_{wc} f_y}{\gamma_{M0}} \tag{4.20}$$

$$F_{t,wb,Rd} = \frac{b_{eff,t,wb} t_{wb} f_y}{\gamma_{M0}} \tag{4.21}$$

Where

$M_{pl,1,Rd}$	is the plastic bending resistance for failure mode 1, see equation (4.22)
$M_{pl,2,Rd}$	is the plastic bending resistance for failure mode 2, see equation (4.23)
e_w	is $d_w/4$, where d_w is the diameter of the washer
$F_{t,Rd}$	is the design tension resistance of a bolt for a bolt, see equation (4.24)
n	is a geometrical dimension describing the position of the prying force. It is the minimum value of e_{min} and $1,25m$
e_{min}	is the smaller distance from the bolt, see figure 4.15
l_{eff1}, l_{eff2}	is the minimum effective lengths to the corresponding failure mode
t_{wc}	thickness of the column web
ω	a reduction factor, see equation (4.25)
$b_{eff,t,wc}$	is the effective width and equal to the effective length of the column flange
$b_{eff,t,wb}$	is the effective width and equal to the effective length of the end-plate

The plastic bending moment and the bolts tension resistance are given in equation (4.22), equation (4.23) and equation (4.24).

$$M_{pl,1,Rd} = \frac{0,25 \sum l_{eff,1} t_f^2 f_y}{\gamma_{M0}} \tag{4.22}$$

$$M_{pl,2,Rd} = \frac{0,25 \sum l_{eff,2} t_f^2 f_y}{\gamma_{M0}} \tag{4.23}$$

$$F_{t,Rd} = \frac{0.9 A_s f_{yb}}{\gamma_{M2}} \tag{4.24}$$

Where

t_f	is the thickness of the T-stub flange
f_y	is the yield strength
A_s	is the tensile stress area of a bolt
l_{eff1}, l_{eff2}	is the minimum effective lengths to the corresponding failure mode

The reduction factor ω is to allow the shear interaction with the column web. ω can be determined by equation (4.25). [Dansk Standard, 2007]

$$\omega = \frac{1}{\sqrt{1+1,3(b_{eff,c,wc}t_{wc}/A_{vc})^2}} \tag{4.25}$$

Two methods are used for the bearing resistance of failure mode 1, where the lowest bearing resistance is used. Method 1 assumes the force from the bolt applied to the T-stub flange is concentrated in the centre-line of the bolt, while the method 2 assumes the force is uniformly distributed under the washer, see figure 4.14. [Dansk Standard, 2007]

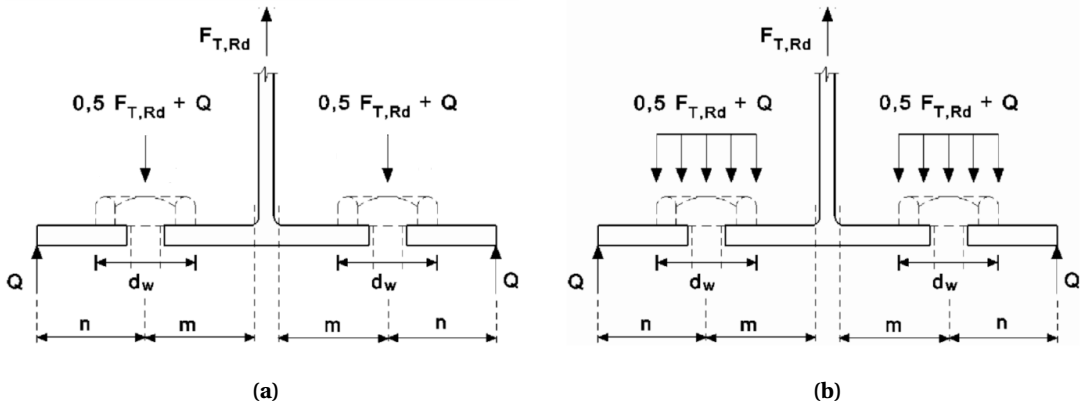

(a) **(b)**

Figure 4.14: Force distribution under the washer of (a) method 1 (b) method 2 for failure mode 1.

The value n is a geometrical length describing the position of the prying force. It is the minimum value of e_{min} and $1,25m$, see figure 4.15.

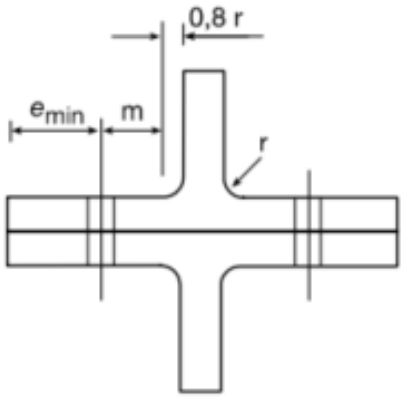

Figure 4.15: Definition of e_{min} and m [Dansk Standard, 2007].

Eurocode 3 Part 1-8 describes another failure mode, where the bolts can elongate significantly, this results in negligible prying force. If no prying forces develops, the design formula for failure mode 1 and 2 is substituted to equation (4.18). [Vayas et al., 2019]

4.1.5 Design resistance of the column web in compression

The design resistance of the column web in compression for an unstiffened joint is given in equation (4.26).

$$F_{c,wc,Rd} = \frac{\omega k_{wc} b_{eff,c,wc} t_{wc} f_y}{\gamma_{M0}} \text{ but } F_{c,wc,Rd} \leq \frac{\omega k_{wc} \rho b_{eff,c,wc} t_{wc} f_y}{\gamma_{M1}} \tag{4.26}$$

Where

ω	is a reduction factor, see equation (4.25)
k_{wc}	is a reduction factor due to the compressive stress in the column and is set equal to 1
ρ	is a reduction factor due to plate buckling

The left hand side expression of equation (4.26) is the resistance of the column web in compression, while the right hand side takes instability into consideration by using ρ which is determined from the plate slenderness $\bar{\lambda}_p$, see equation (4.27).

$$\bar{\lambda}_p = 0,932\sqrt{\frac{b_{eff,c,wc} d_{wc} f_y}{E t_{wc}^2}} \text{ if } \left\{ \begin{array}{c} \bar{\lambda}_p \leq 0,72 \ , \ \rho = 1,0 \\ \bar{\lambda}_p > 0,72 \ , \ \rho = (\bar{\lambda}_p - 0,2)/\bar{\lambda}_p \end{array} \right\} \tag{4.27}$$

Where

d_{wc}	is equal to $h_c - 2(t_{fc} + r_c)$
E	is the Youngs modulus
r_c	is the root fillet

The resistance for the column web in compression is compared to the total tension resistance. If the tension resistance is greater than the compression resistance the tension resistance is reduced.

4.1.6 Design resistance of the web panel in shear

For a single sided joint, the design plastic shear resistance $V_{wp,Rd}$ for an unstiffened column web panel is given in equation (4.28).

$$V_{wp,Rd} = \frac{0,9 f_y A_{vc}}{\sqrt{3}\gamma_{M0}} \tag{4.28}$$

Equation (4.28) is only valid if the column web slenderness satifies the condition $d_{wc}/t_{wc} \leq 69\epsilon$. The resulting shear force from the bending moment for a single sided joint is obtained with equation (4.29). The forces are shown in figure 4.16.

$$V_{wp,Ed} = \frac{M_{Ed}}{z} - V_{Ed} \tag{4.29}$$

Where

ϵ	is equal to $\sqrt{f_y/235\text{MPa}}$ [Dansk Standard, 2022]
A_{vc}	is the shear area of the column
z	is the lever arm, see figure 4.17

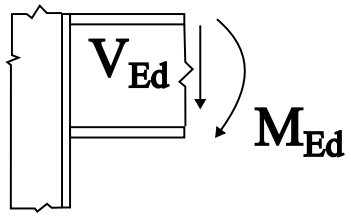

Figure 4.16: Illustration of the lever arm.

There is not applied any shear force, so only the bending moment will affect the web panel. The lever arm, z is shown in figure 4.17 and given as the distance from the centre of compression to the midway point between the two bolt-rows.

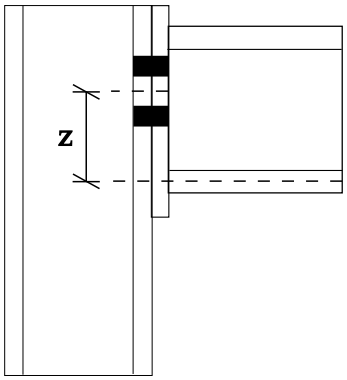

Figure 4.17: Illustration of the lever arm.

4.2 Moment bearing capacity from the Component Method

With the known effective lengths for each component and whether prying forces develops, the bearing capacity can be determined for the relevant components with equation (4.15) to equation (4.21). The bearing capacity is determined for each basic component and considering bolt-rows as individual and in a group of bolt-rows. The design resistance for each basic component will then consist of three resistances, see equation (4.30).

$$F_{t,i,Rd} = \begin{bmatrix} \min(F_{t,i,r1,Rd}) \\ \min(F_{t,i,r2,Rd}) \\ \min(F_{t,i,r1-2,Rd}) \end{bmatrix} \tag{4.30}$$

Where:

$F_{t,i,Rd}$	is the design resistance for the basic component i
$F_{t,i,r,Rd}$	is the design resistance for bolt-row r of basic component i

The sum of the individual bolt-rows design resistance must be lower than the design resistance of the group of bolt-rows [Dansk Standard, 2007], so equation (4.31) must be fulfilled.

$$F_{tr1-2,Rd} \geq F_{tr1,Rd} + F_{tr2,Rd} \tag{4.31}$$

If equation (4.31) is not fulfilled, the design resistance for the bolt-row closest to the centre of compression is reduced until it is fulfilled. [Dansk Standard, 2007]

The design resistances from each of the basic components are compared and the joints bearing capacity is then taken as the minimum value of all the basic components individual bearing resistance, see equation (4.32).

$$F_{tr,Rd} = \begin{bmatrix} \min(F_{tr1,Rd}) \\ \min(F_{tr2,Rd}) \\ \min(F_{tr1-2,Rd}) \end{bmatrix} \tag{4.32}$$

The moment bearing resistance $M_{j,Rd}$ can then be determined from equation (4.1).

4.3 Rotational stiffness

The rotational response of the joint is determined from the rotational stiffness of the joint given in equation (4.33). It is determined from the flexibility's of the basic components. The basic components flexibility's are represented by the stiffness coefficients k_i. [Dansk Standard, 2007]

$$S_j = \frac{Ez^2}{\mu \sum \frac{1}{k_i}} \tag{4.33}$$

Where:

z	is the lever arm, see figure 4.17
k_i	is the stiffness coefficient of the basic component i
μ	is the stiffness ratio between the linear and non-linear curve, see figure 3.2

The stiffness coefficient of each the basic components are described at the beginning of chapter 4. They can be determined according to EC3 Part 1-8 and is given in equation (4.34) to equation (4.39). The expressions are developed through experimental and numerical research [Weynand et al., 1995].

$$k_1 = \frac{0,38A_{vc}}{\beta z} \quad \text{Column web panel in shear} \tag{4.34}$$

$$k_2 = \frac{0,7b_{eff,c,wc}t_{wc}}{d_c} \quad \text{Column web in compression} \tag{4.35}$$

$$k_3 = \frac{0,7b_{eff,t,wc}t_{wc}}{d_c} \quad \text{Column web in tension} \tag{4.36}$$

$$k_4 = \frac{0,9l_{eff,flange}t_{fc}^3}{d_c} \quad \text{Column flange in bending} \tag{4.37}$$

$$k_5 = \frac{0,9l_{eff,ep}t_p^3}{m^3} \quad \text{End-plate in bending} \tag{4.38}$$

$$k_{10} = \frac{1,6A_s}{L_b} \quad \text{Bolts in tension} \tag{4.39}$$

Where:

A_{vc}	is the shear area of the bolt according to Eurocode 3 Part 1-1
β	is the transformation parameter and is equal to 1 for a single sided joint connection
$b_{eff,c,wc}$	is the effective width of the column web in compression component
$b_{eff,t,wc}$	is the effective width of the column web in tension component
d_c	is the inner distance from flange to flange
t_{wc}	is the thickness of the column web
t_{fc}	is the thickness of the column flange
m	is defined in figure 4.15

$b_{eff,c,wc}$ for a bolted end-plate connection is determined from equation (4.40). $b_{eff,t,wc}$ is equal to the smallest effective length l_{eff} given from figure 4.10.

$$b_{eff,c,wc} = t_{fb} + 2\sqrt{2}a_p + 5(t_{fc} + s) + s_p \tag{4.40}$$

Where:

s_p	is the length obtained by dispersion of 45° through the end-plate
$\sqrt{2}a_p$	is the leg-size of the weld connection
s	is the root radius of an I- or H section

With the known stiffness coefficients of the equivalent stiffness coefficient k_{eq} can be determined from equation (4.41).

$$k_{eq} = \frac{\sum_r k_{eff,r}h_r}{z_{eq}} \tag{4.41}$$

Where:

$k_{eff,r}$	is the effective stiffness coefficient for bolt-row r taking the stiffness coefficient k_3, k_4, k_5 and k_{10} into account
h_r	is the distance from bolt-row r to the centre of compression
z_{eq}	is the equivalent lever arm

The effective stiffness coefficient $k_{eff,r}$ is determined from equation (4.42).

$$k_{eff,r} = \frac{1}{\sum_i \frac{1}{k_{i,r}}} \tag{4.42}$$

Where:

$k_{i,r}$	is the stiffness coefficient of component i for bolt-row r

The equivalent lever arm z_{eq} is determined from equation (4.43).

$$z_{eq} = \frac{\sum_r k_{eff,r} h_r^2}{\sum_r k_{eff,r} h_r} \tag{4.43}$$

The stiffness ratio μ is used to dictate the varying stiffness in the non-linear part of the rotational response. The stiffness ratio is determined from the following:

$$\mu = 1 \qquad \text{if } M_{j,Ed} \leq 2/3 M_{j,Rd} \tag{4.44}$$

$$\mu = \left(\frac{1,5 M_{j,Ed}}{M_{j,Rd}}\right)^{\psi} \qquad \text{if } M_{j,Ed} > 2/3 M_{j,Rd} \tag{4.45}$$

The value ψ is a constant and determined from Eurocode 3 Part 1-8 and is equal to 2,7 for a bolted end-plate. From the given equations the rotational stiffness of the joint can be calculated with equation (4.33). With the stiffness known the rotational response can be determined.

4.4 Results

The calculated initial stiffness's and moment bearing capacities of the models are stated in table 4.1. A worked example is shown in appendix B. The column and beam profiles are kept constant as HE240B and IPE200 respectively while the end-plate thickness is changed.

	End-plate thickness, t_{ep} [mm]	Initial stiffness, $S_{j,ini}$ [kNm/(°)]	Moment bearing capacity, $M_{j,Rk}$ [kNm]
Model 1	10	3,05 10^3	20,23
	14	3,85 10^3	25,59
	17	4,08 10^3	32,32
Model 2	10	3,90 10^3	24,35
	14	5,56 10^3	29,38
	17	6,06 10^3	29,38
Model 3	10	5,00 10^3	23,11
	14	5,11 10^3	28,35
	17	5,10 10^3	28,35
Model 4	10	2,70 10^3	20,34
	14	3,53 10^3	25,81
	17	3,81 10^3	27,98

Table 4.1: Moment bearing capacity of the models and different end-plates.

From table 4.1 it is evident that Model 2 and 3 has a significant greater moment bearing capacity. The models are the ones with the bolts placement furthest from the centre-line of compression, which could lead to a greater bearing capacity. The moment-rotation curves are shown in figure 5.8, figure 5.10 and figure 5.11.

5. FEM modelling of a joint

The purpose of this chapter is to model and analyse the different joint configurations in ANSYS. The FE models are presented and a convergence analysis is conducted for one of the models.

The idea of modelling with FEM is to subdivide a large model into smaller parts, also called finite elements which each contains a number of nodes. It is through these nodes that a solution is found in regards to the proposed problem. The software used is ANSYS and the element type used is SHELL181 which is a 4-node shell element. Each node has 6 degrees of freedom (DOFs), three of them being translational in the x, y and z direction and three being rotational degrees of freedom around the $x-$, $y-$ and $z-$axis. The element is shown in figure 5.1.

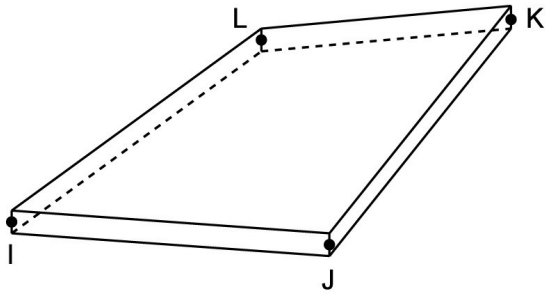

Figure 5.1: Illustration of the element SHELL181. [ANSYS, 2023b]

The full model is not modelled as the provided version of ANSYS is a STUDENT version and can only solve problems with a limited number of DOFs of 128.000 nodes. Therefore the model is reduced to figure 5.2 as only the internal moment at the joint is in interest for the moment bearing capacity. This provides a denser mesh compared to modelling the full-scale frame, which in turn can provide with more precise results.

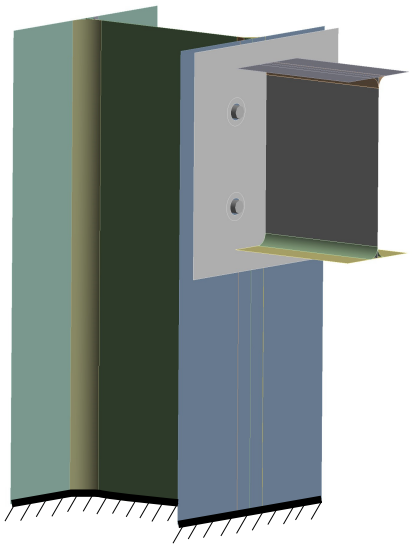

Figure 5.2: Illustration of the reduced model and the support condition used for the numerical model.

The bolts are modelled as a beam element instead of a solid element. This can reduce the computational time as modelling the bolts, header and washer can increase the number of elements and nodes. The beam element is scoped between two holes and connected to an area the size of the washer, see figure 5.3 (a). The beam connection consists of two nodes (I and J), see figure 5.3 (b). The two nodes are pilot nodes and each node has 6 DOFs with 3 being translational and 3 being rotational. The connections between the beam connections and the area of the washer is done through the pilot node, see figure 5.3 (c). The multipoint constraints applies kinetic constraints, which are infinitely stiff elements, between the pilot nodes and the nodes at the washer, see figure 5.3 (d). [ANSYS, 2023a]

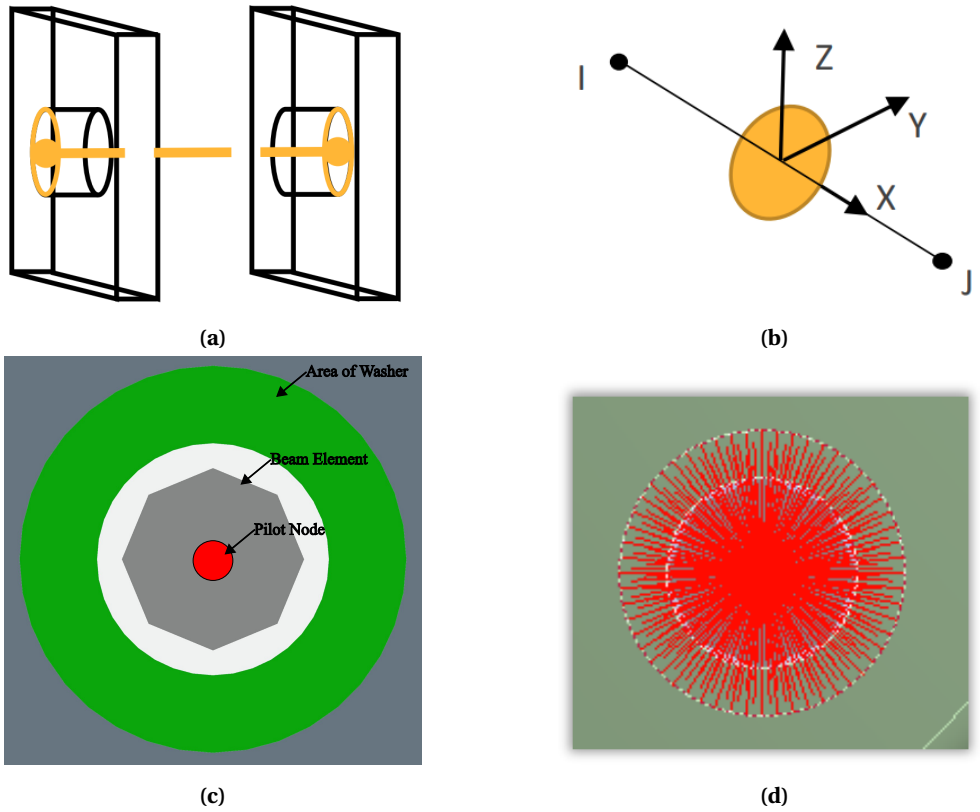

Figure 5.3: Illustrations of (a) A beam element connection (b) non-circular yield patterns (c) the the pilot node of the bolt and the washer, which are connected (d) the kinetic constraints between the pilot node and the washer. [ANSYS, 2023a]

The weld is not considered and therefore the beam and end-plate are connected with use of shared topology. The area where the beam and end-plate are in contact, the nodes are shared and therefore the beam and end-plate act as one element. This ensures that they won't separate. The contact area between the end-plate and column flange are modelled as a frictionless contact. This establishes a contact where both elements can separate and hinders the elements topology merging under er loading condition.

The support condition is seen in figure 5.2. This is the general model used to model the joints. The bolt placement and end-plate thickness are changed for each of the models. The material model is described in chapter 2.2.

5.1 Numerical model

The numerical model in ANSYS consist of an assembly of the column flange and an end-plate which is welded to the beam. A set of bolts then connects the end-plate and column flange. The individual components are shown in figure 5.4 and the meshed models are shown in figure 5.5.

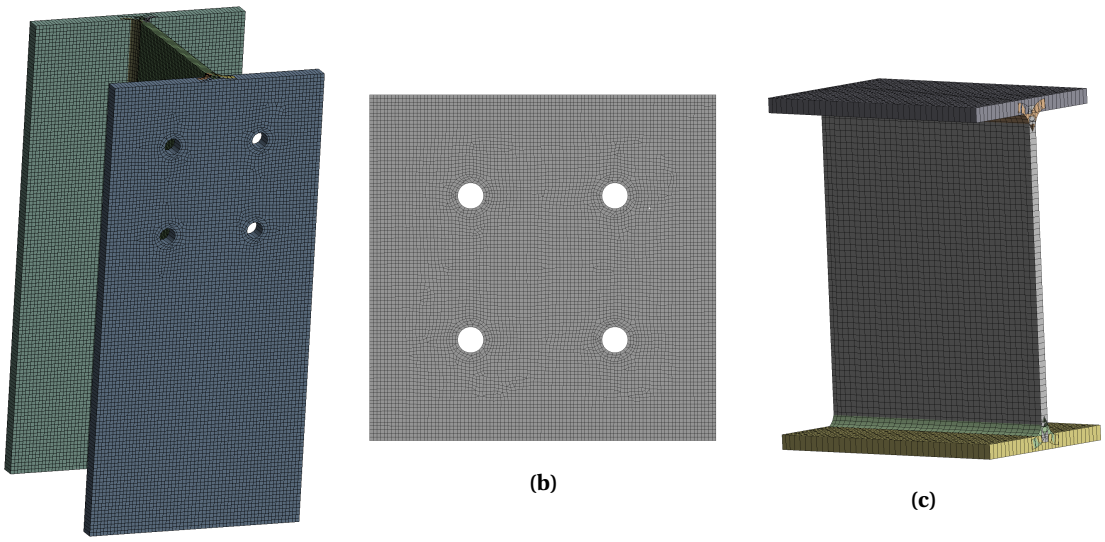

(a) **(b)** **(c)**

Figure 5.4: Illustation of the individuel components.

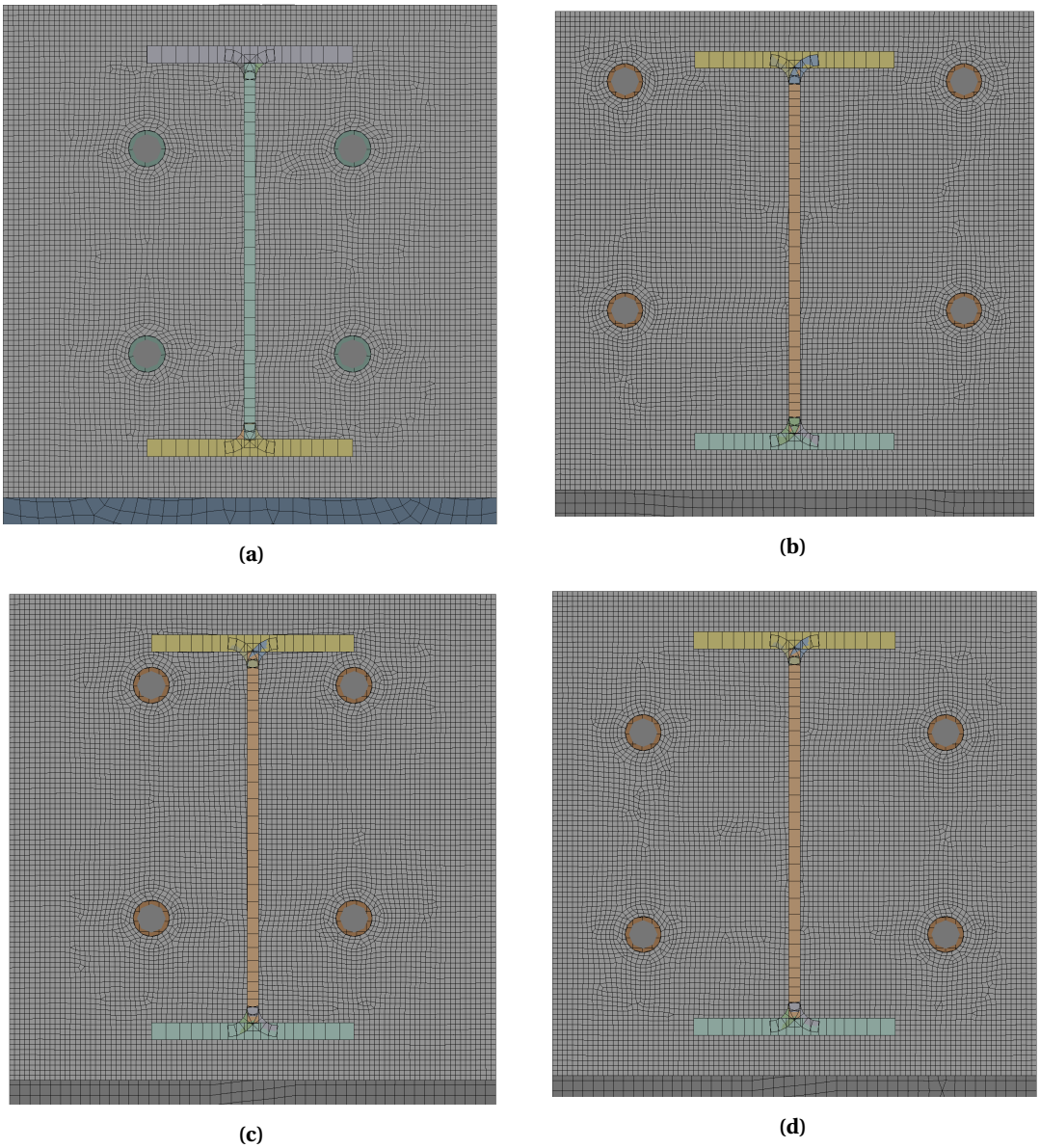

Figure 5.5: The mesh for (a) Model 1, (b) Model 2, (c) Model 3 and (d) Model 4.

The bending moment is established at end of the beam, see figure 5.6 (a), and is increased in increments. The finite element software uses the Newton-Raphson method to converge towards a solution, which is a iterative method to obtain the corresponding displacements and deformation at a given load step. This method is further explained in appendix C. Load control is used since the bending moment is controlled and for each load increment the displacement are calculated. Displacement control is not applicable in this model, as ANSYS cannot introduce a rotational displacement. In principle both methods should give the same results, but displacement control tend to be more stable and can lead to more precise results. [Krenk, 2009] [Cook et al., 2002]

The rotation is simplified to a linear rotation and calculated by using the trigonometry of a right triangle whereas the displacement is calculated at the top and bottom flange. The displacement

is obtained at the points seen in figure 5.6 (b) indicated with an "x" at the connection between the end-plate and beam. The deformed joint is shown in figure 5.12, where the deformed end-plate is non-linear and therefore assuming it to be linear is a simplification of the deformed joint.

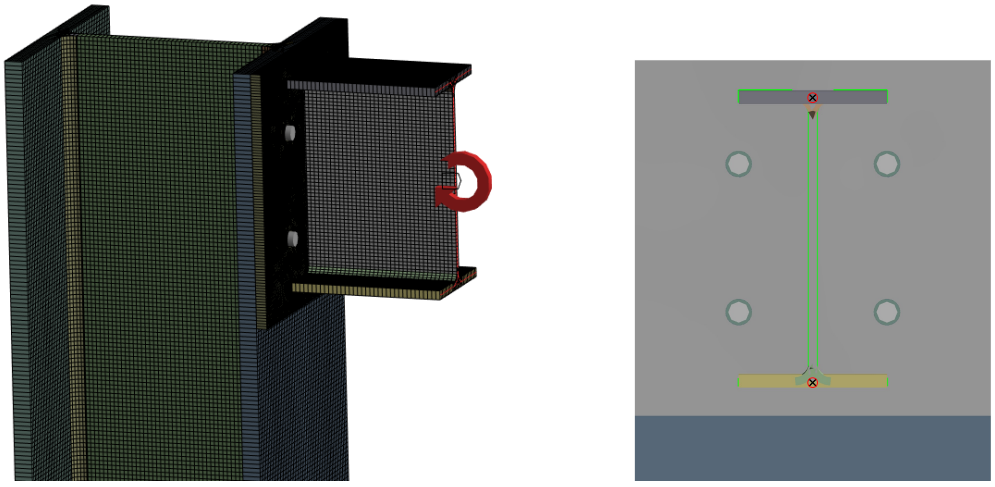

(a) **(b)**

Figure 5.6: (a) is a illustration of where the bending moment is established (b) is a frontal view where the "x" indicates where the displacement is obtained.

The rotational deformation is obtained by using equation (5.1).

$$\theta = \arctan\left(\frac{d_1 + d_2}{h_1}\right) \tag{5.1}$$

Where:

d_1	is the displacement at the top flange point
d_2	is the displacement at the bottom flange point
h_1	is vertical distance between the two points

5.2 Convergence

For a numerical model a convergence analysis needs to be carried out, to determine if the model has a sufficient mesh. The convergence analysis is done to Model 1 with an end-plate thickness of 10 mm within the elastic region of the material model. A moment force is applied to the end of the beam of $M_j = 15$ kNm. The convergence is illustrated in figure 5.7.

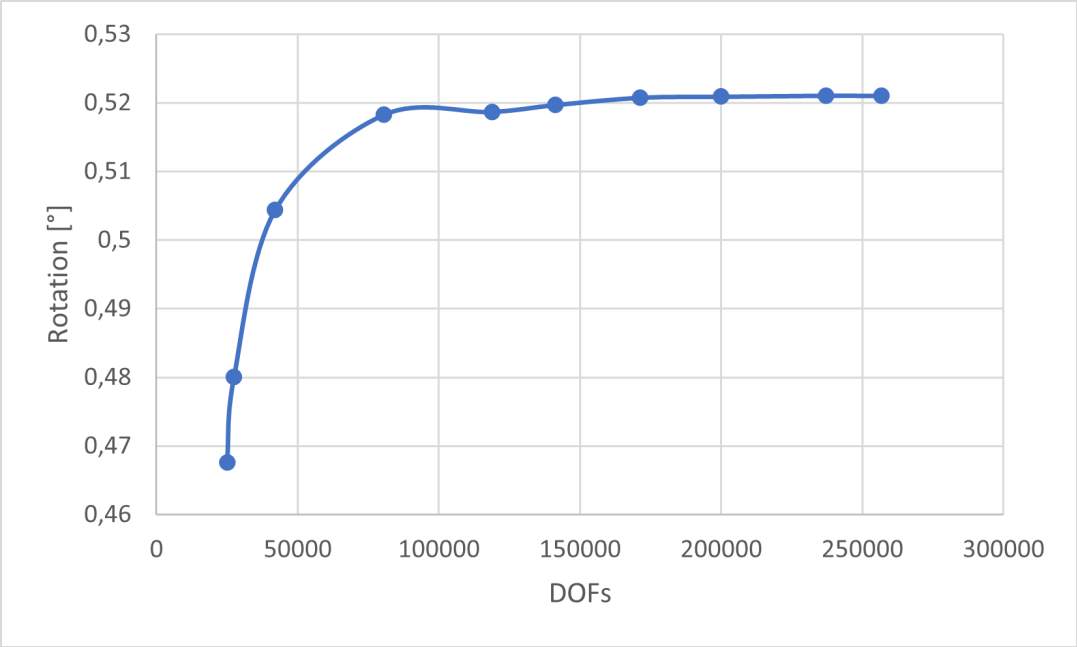

Figure 5.7: The rotation at the beam-end-plate connection compared to the number of DOFs for model 1.

The STUDENT license of ANSYS has a limited amount of nodes/elements of 128 000 and therefore limits the mesh sensitivity. The computational time at the lower amount of DOFs is around 15 seconds, while at the higher amount of DOFs could take up to 45 minutes. Therefore choosing a lower number of DOFs can significantly decrease the computational time when also performing a non-linear analysis. It can be observed in figure 5.7 that a convergence is reached at around 150 000-200 000 DOFs and it is within this span the other models are modelled as well.

5.3 Results and comparison

The moment bearing capacity determined from the Component Method and numerical model are compared. The models for which the moment bearing capacity is determined are shown in figure 5.5 and described in chapter 2. Figure 5.8, figure 5.10 and figure 5.11 shows the moment-rotation, $M-\theta$, curves for three different end-plate thickness. The Component Method is explained in chapter 4 and the numerical model is described in chapter 5. Figure 5.8 shows the rotational response to of Model 1-4 with and end-plate thickness of 10 mm. The linecolour represents the model and linetype represents the method of analysis.

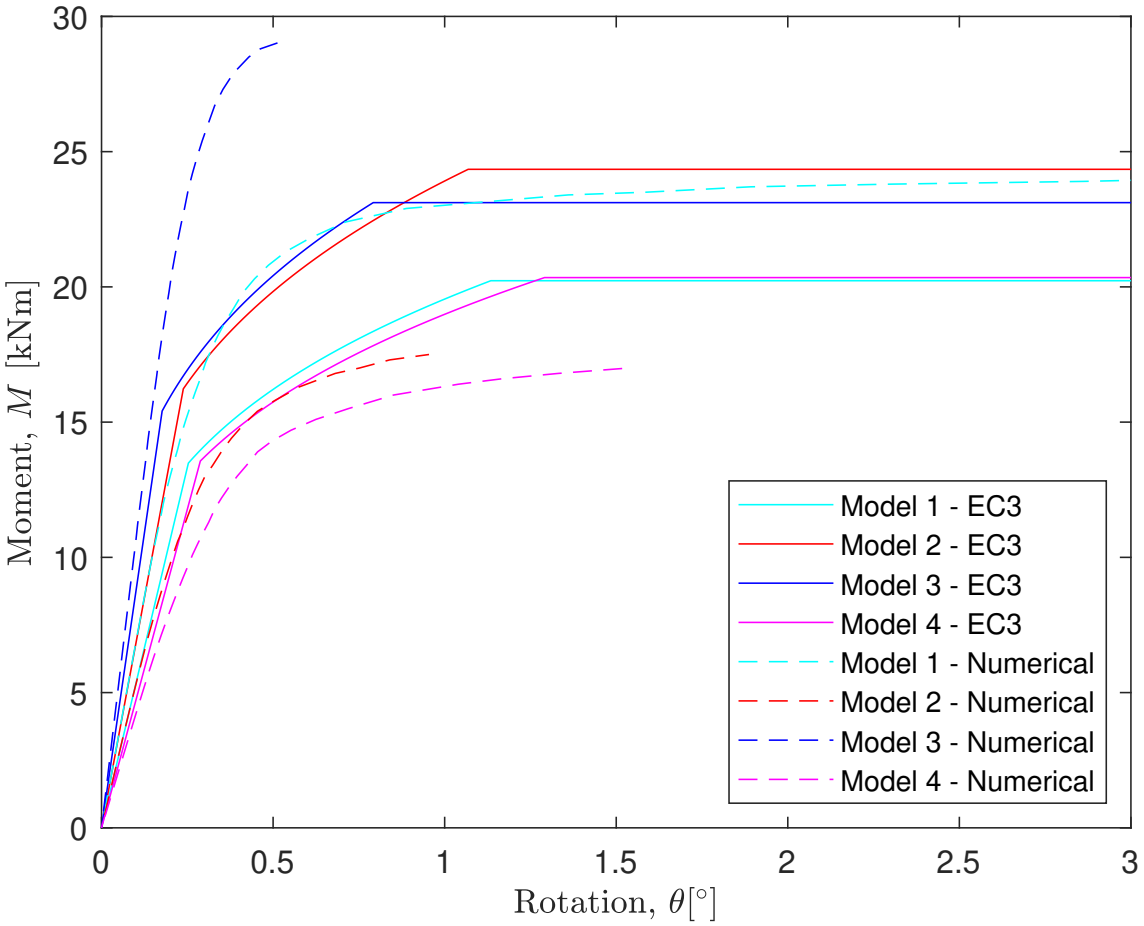

Figure 5.8: Comparison of the four joint configurations with end-plate trickiness of 10 mm.

Figure 5.8 strongly indicates a discrepancy between the Component Method and the numerical method for certain joint configurations. The numerical model of Model 2 and Model 4 shows a large discrepancy compared to the Component Method with a lower moment bearing capacity. This is likely due to the placement of the bolts being close to the edge of the end-plate. The equivalent Von-Mises stresses at the surface of the end-plate are illustrated in figure 5.9(a) and figure 5.9(b) at approximately 50 % of the largest bending moment for the numerical model of Model 1 and Model 2 respectively. It shows that the formation of the stresses around the upper boltholes are reaching the materials yield stresses for both cases, although yielding occurs at edge of the end-plate for Model 2. This can result in a lower bearing capacity as the stresses around the bolt-hole cannot redistribute as effectively compared to a model where the boltholes are further from the edge. It can further be examined that numerical model of Model 1 and Model 3 has a greater moment bearing capacity than the Component Method.

Figure 5.10 shows the $M-\theta$-curve for the end-plate being 14 mm. The rotational response of the numerical model of Model 2 and Model 4 are closer to the rotational response of the Component Method. It is clear that an increase in end-plate thickness results in a larger moment bearing resistance of the numerical model compared to the Component Method.

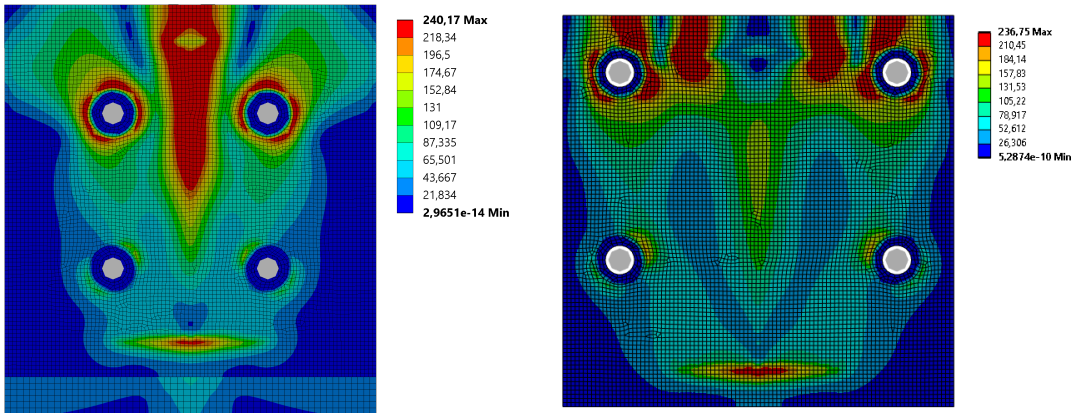

(a) **(b)**

Figure 5.9: Equivalent Von-Mises stresses for (a) Model 1 end-plate with thickness of 10 mm and (b) Model 2 with end-plate thickness of 10 mm at $M = 11,5$ kNm.

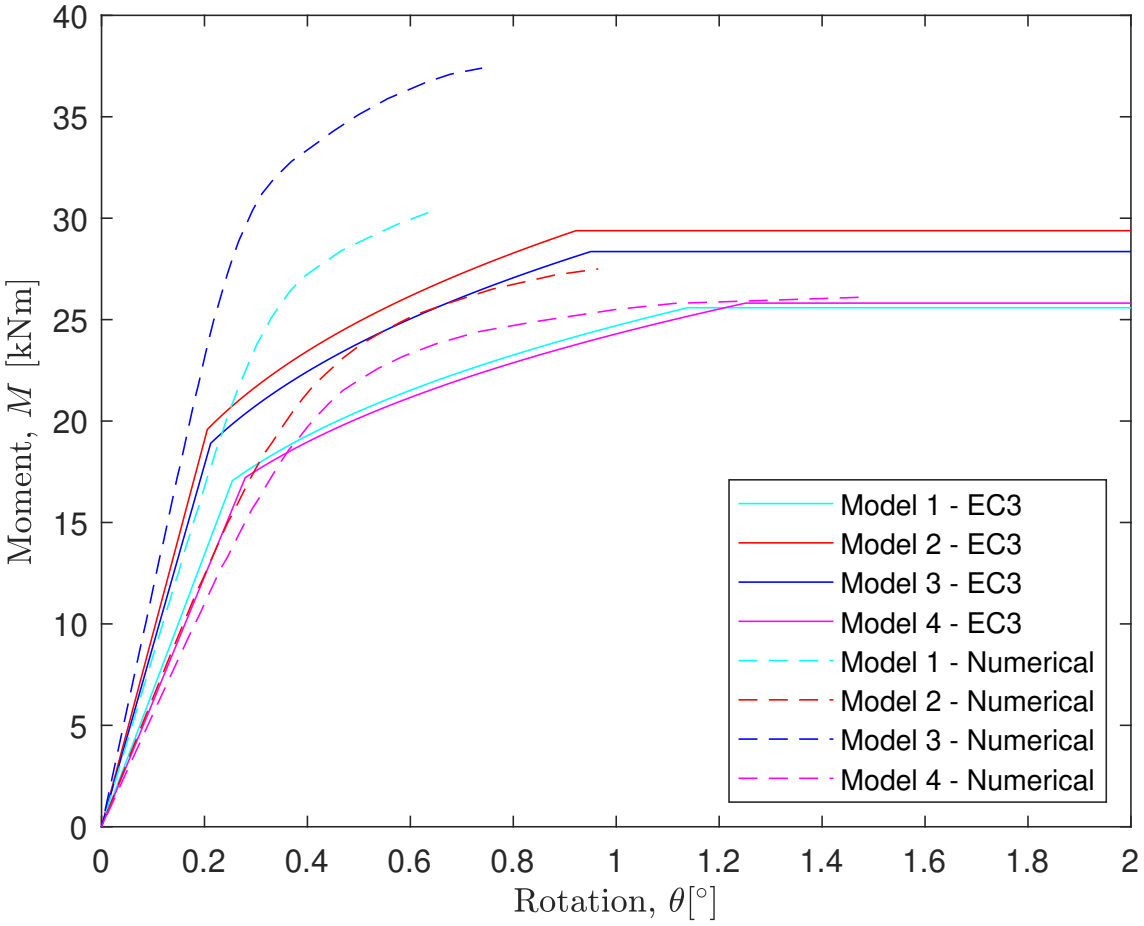

Figure 5.10: Comparison of the four joint configurations with end-plate trickiness of 14 mm.

The rotational response of the end-plate thickness of 17 mm is seen in figure 5.11. It can be seen that the numerical model for Model 2 shows a moment bearing capacity lower than the other models. For the other 3 models, the moment bearing capacity determined with the numerical

model is shown to be greater, as a larger bending moment is required for a similar rotational response for the Component Method.

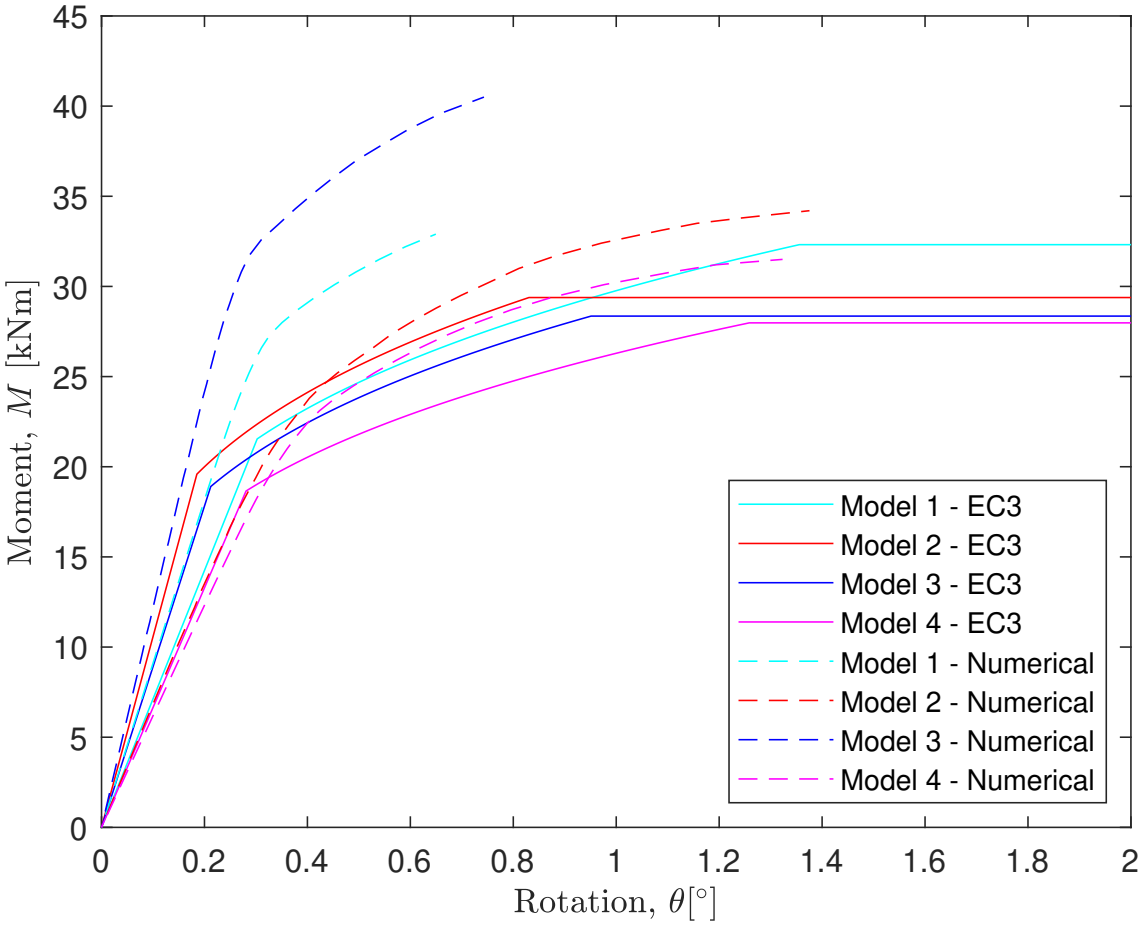

Figure 5.11: Comparison of the four joint configurations with end-plate trickiness of 17 mm.

The deformed joint of Model 1 with end-plate thickness of 10 mm is seen in figure 5.12. Figure 5.12 (a) shows the deformed joint at half the largest moment and figure 5.12(b) and it can be seen that the structure deforms as expected. The beam and end-plate does not separate and establishes a contact region between the end-plate and the column flange.

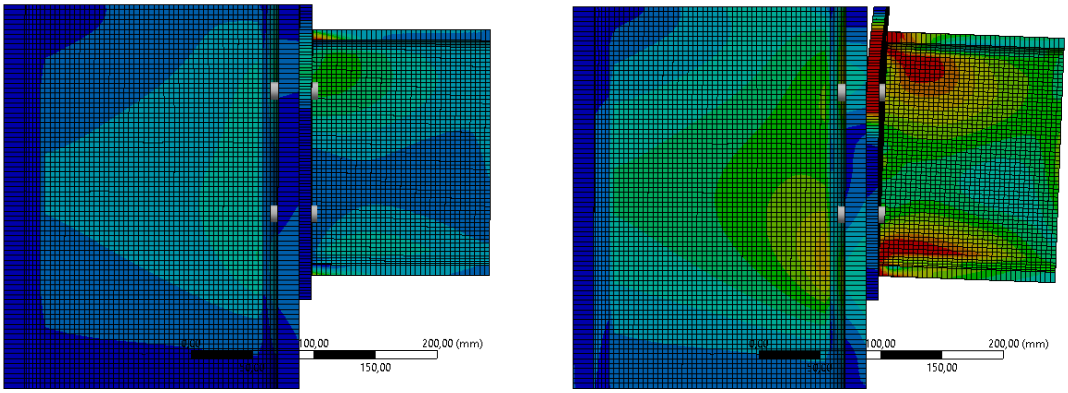

(a) **(b)**

Figure 5.12: The deformed joint of Model 1 with end-plate thickness of 10 mm at (a) 50% of the largest applied moment (b) the end of the simulation.

III Moment distribution

6. Analysis of frame

This chapter introduces the frame which the bending moment distribution is determined. The points where the bending moment is determined are showed.

The considered frame is illustrated in figure 6.1 and is analysed in 2D in both the analytical and numerical model. Due to symmetry, the moments at the two supports are equal as well as the moment at the two joints. Therefore only point A, B and C are considered when determining the moment distribution. The circle with the "x" indicates the joint with rotational springs. Point C is at the centre of the beam. The dimensions of the beam and columns are listed in table 2.2.

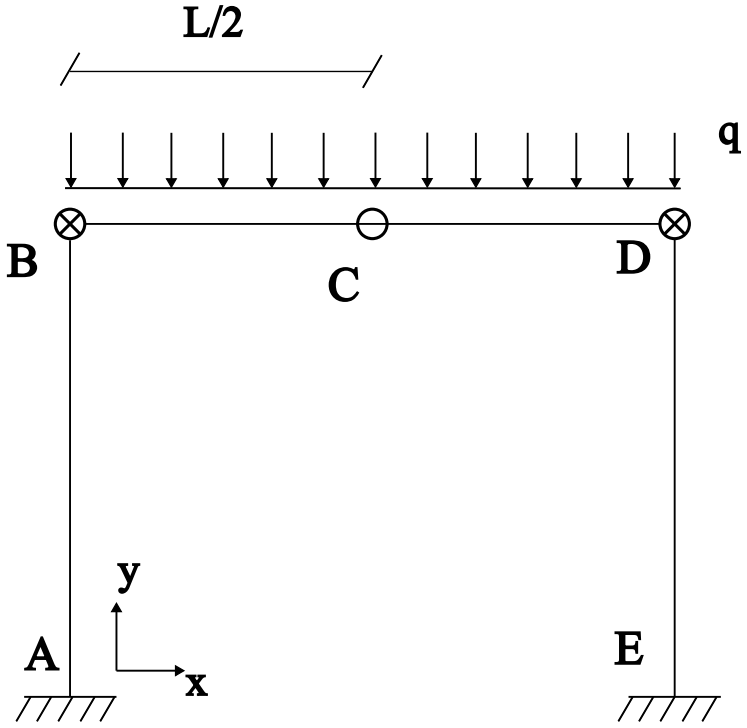

Figure 6.1: Illustration of the static system.

The moment at point A, B and C are determined with varying joint stiffness's from the joint assumed pinned to rigid. The bending moment distribution of the considered frame, when the joints are assumed pinned, rigid and semi-rigid are shown in figure 6.2.

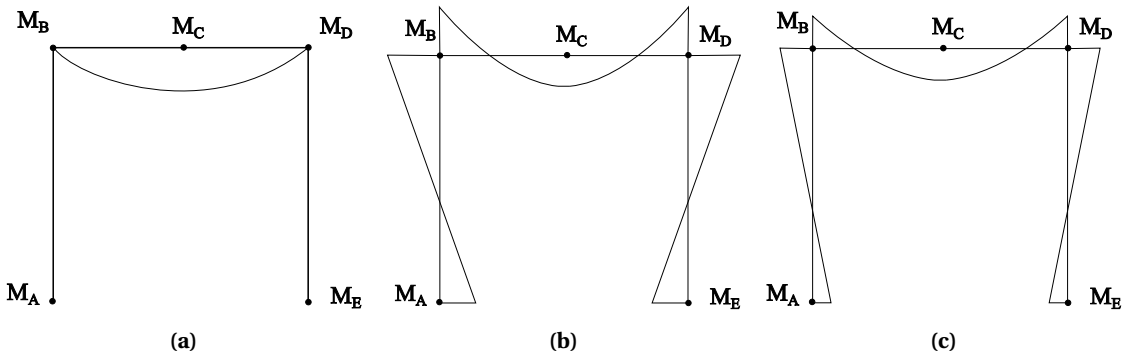

Figure 6.2: Principle sketches of the bending moment diagram of a frame with (a) rigid joints (b) pinned joints (c) semi rigid joints.

The bending moment diagram in figure 6.2 shows the bending moments of the considered frame when the joints are considered rigid and pinned. It can be seen that the bending moment at the point of interest are local maxima.

The analytical and numerical models are compared to validate the results. The moments at point A, B and C are compared and the non-linear moment-rotation curves from chapter 5.3 are then used to establish the relation between the bending moment at the joint and the load q shown in figure 6.1.

7. Analytical model

In this chapter the analytical method to determine the bending moment distribution is used. The analytical method used is the slope-deflection method. The rotational stiffness of the beam-to-column joint is changed, and the bending moment distribution is determined at the locations specified in chapter 6. The derivation of the Kleinlogel-type formulations are expanded on in appendix D.

The slope-deflection method is used to determine the moment distribution of the frame given in 6.1. The slope-deflection method is a method to obtain the end-moments of statically indeterminate structures and was first used for analysis of rigid-joint structures [Norris et al., 1997]. The expressions for the end-moments are derived from rotations and deflection of the joint and is a linear elastic method [McCormac and Nelson, 1997]. Adolf Kleinlogel authored a book which contained formulas that determined the internal bending moments and forces for rigid frames under different loading conditions. The formulas were produced using elastic analysis with only bending causing deformations and was obtained using the slope-deflections equations [Kleinlogel, 1953]. Kleinlogel simplified the formulas by introducing notations, which were specific for a frame with a specific loading scenario [Henderson, 2022].

Kleinlogel's formula for a portal frame shown in figure 6.1 with fixed support and rigid joints, have been modified so it includes joint stiffness's. The bending moment at the support is given in equation (7.1) and the bending moment at the joints is given in equation (7.2), see appendix D for the method of obtaining the formulas. The formulations are derived and expressed as a Kleinlogel-type formulae. [Henderson, 2022]

$$M_A = \frac{qL^2}{12}\frac{(1-2K_A)K_B}{(2-K_A+kK_B)} \tag{7.1}$$

$$M_B = -\frac{qL^2}{12}\frac{(2-K_A)K_B}{(2-K_A+kK_B)} \tag{7.2}$$

K_A and K_B are coefficients which are dependent on the stiffness of the column feet and joint respectively. They are determined from equation (7.3).

$$K_A = \frac{2EI_c}{S_{jA}H+4EI_c};\ K_B = \frac{S_{jB}H}{S_{jB}H+2kEI_c} \tag{7.3}$$

Where:

k	is equal to $\frac{I_b H}{I_c L}$
I_c	is the columns moment of inertia
I_b	is the beams moment of inertia
S_{jA}	is the rotational stiffness of the support
S_{jB}	is the the rotational stiffness of the joint
H	is the height of the frame
L	is the length of the frame

When the end-moments are known, the bending moment at point C can be determined using equation (7.4). The derivation is shown in appendix E.

$$M_C = M_B + \frac{q(L/2)^2}{2} - \frac{qL}{2} \tag{7.4}$$

The rotational stiffness at the support S_{jA} is infinite as the support is assumed fixed. The coefficient K_A will then be equal to 0 and therefore does not influence the bending moment distribution of the frame when the joints rotational stiffness are changed. The slope-deflection method assumes the centre-lines of the beam and column are connected with no eccentricities, see figure 8.2 (a).

The bending moments determined from equation (7.1), equation (7.2) and equation (7.4) can be normalised with the distributed load q as the model is linear elastic. The results of the analytical model are shown in chapter 8.2.

8. Numerical model

The frame is modelled in RFEM to determine the bending moment distribution at different rotational stiffness' of the joint. Two models are evaluated, one of which introduces an eccentricity at the beam-to-column joint, the other assumes no eccentricities. The results of the numerical model are compared to the result obtained from the analytical model.

The software used to for the numerical modelling is RFEM. The element type is a 2 node elements with 12 DOFs and is used to represent beams, trusses, ribs, cables and rigid couplings. Each node consists of 6 DOFs for translational ind the x-, y- and z-direction and rotations around the x-, y-, and z-axis, see figure 8.1. [Dlubal, 2022]

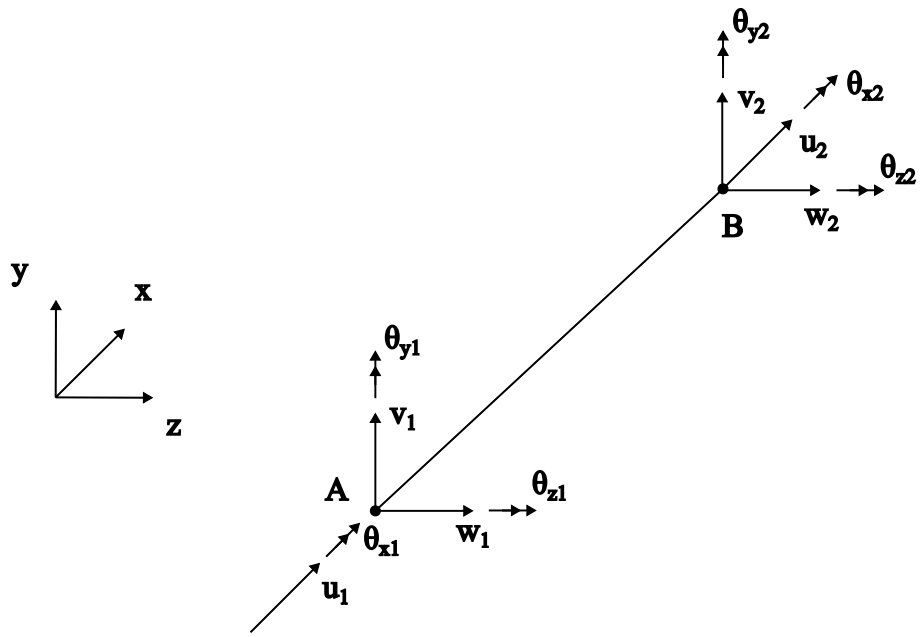

Figure 8.1: Illustration of the elements used in RFEM and the DOFs.

The model is first used as a linear elastic model, where the relation between the bending moments and distributed forces are linear. This is done to validate the numerical model by comparing it to the analytical model. After the numerical model has been validated, the non-linear moment-rotation curves from chapter 5.3 are used to simulate the bending moments at a given load q and compared to the analytical model using a linear elastic material model, to further validate the two models. The load q is gradually increased and a solution is obtained using Newton-Raphson iterations. Newton-Raphson are further expanded on in appendix C. The material model is changes to the one described in chapter 2 and the relation between the bending moment and the load q is determined.

8.1 Modelling of frame

Two models are developed. The first models connects the centre lines of the beam and column and the second which introduces an eccentricity which represents a practical joint more closely. The eccentricity is introduced by transforming the DOFs in the local stiffness matrix for which an infinitely stiff beam connects the end-points of the beam and column [Dlubal, 2023b]. The model where the centre-lines connects represents the analytical model. The moment distributions are determined for both cases. The joints are illustrated in figure 8.2.

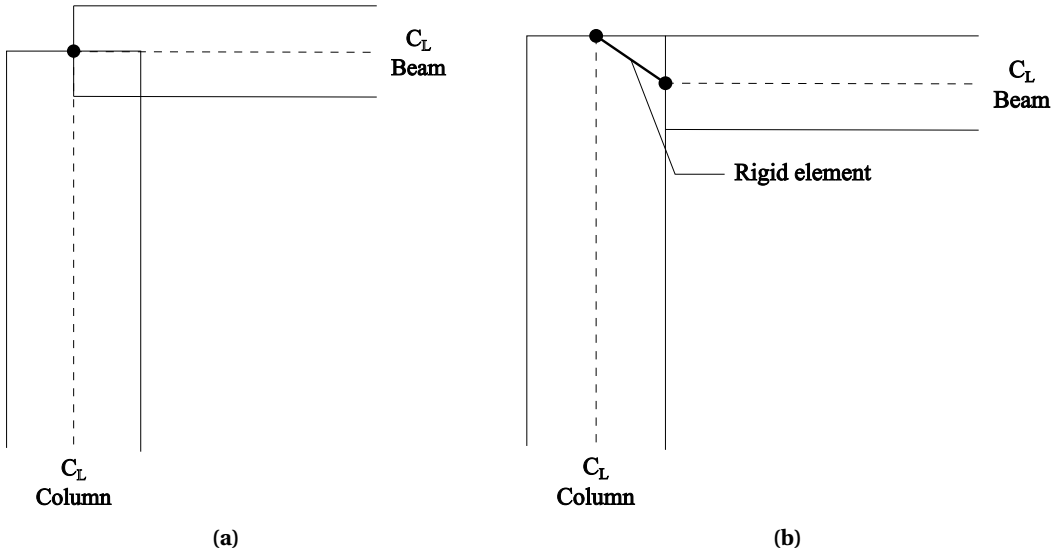

Figure 8.2: Illustration of the two models in RFEM with (a) joint with no eccentricities (b) joint with eccentricities. The rigid element is modelled as infinitely stiff beam.

The stiffness of the joints are analysed from being pinned to fixed and the bending moment at the support, joint and the beam midpoint are measured in the numerical model. Since the relation between the distributed force and the bending moment are linear-elastic, the bending moments can be normalised with the distributed load q. The results are shown in chapter 8.2.

8.2 Results and comparison

The results are the normalised bending moment as a function of the initial stiffness. The results are shown in figure 8.3. The figure shows that the normalised bending moment at Point A, which is the support, determined analytical and numerical are identical. The numerical model which includes the joint eccentricities shows a larger bending moment, while the analytical model closely resembles the numerical model without any joint eccentricities. The normalised bending moment at Point B, which is the joint, shows a larger bending moment with the numerical model with the joint eccentricity. The bending moment from the analytical model and the numerical model with no joint eccentricities are also identical. The bending moments for the numerical model with joint eccentricity follows the same bending moment development with increasing stiffness up until a stiffness of around $3500 kNm/°$. The normalised bending moment at Point C, which is at the middle of the beam, the bending moment for the numerical model with joint

eccentricity is greater than the other two models. The bending moment for the numerical model with the joint with no eccentricities is also identical.

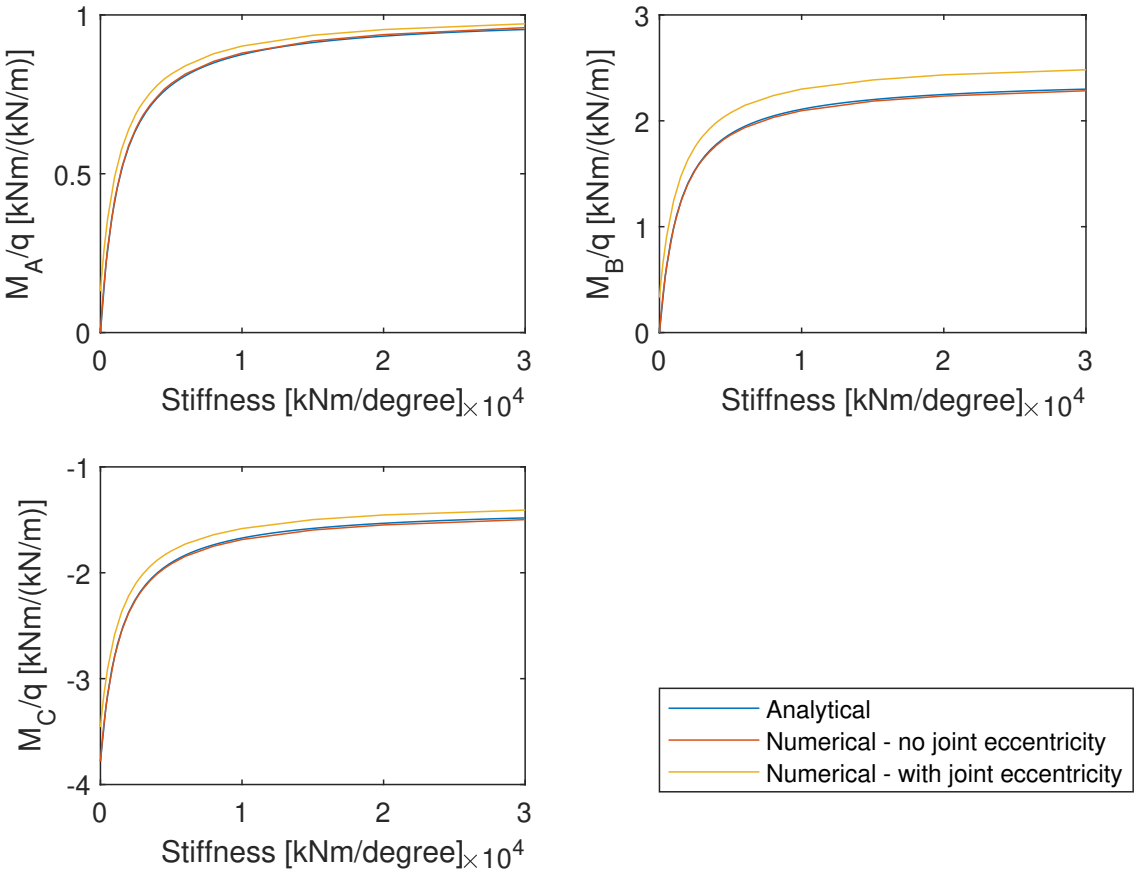

Figure 8.3: The relation between the normalised bending moment distribution and the initial joint stiffness at Point A, B and C.

The non-linear $M-\theta$ curve determined from the moment bearing resistance in chapter 5.3, is used to compare the analytical model and the numerical model with no joint eccentricity. Using the $M-\theta$ curve to represent the joint behaviour under er loading shown in figure 6.1, the load q can be determined for the given bending moment. Figure 8.4 shows the analytical and numerical model, where the numerical model uses a linear-elastic material model.

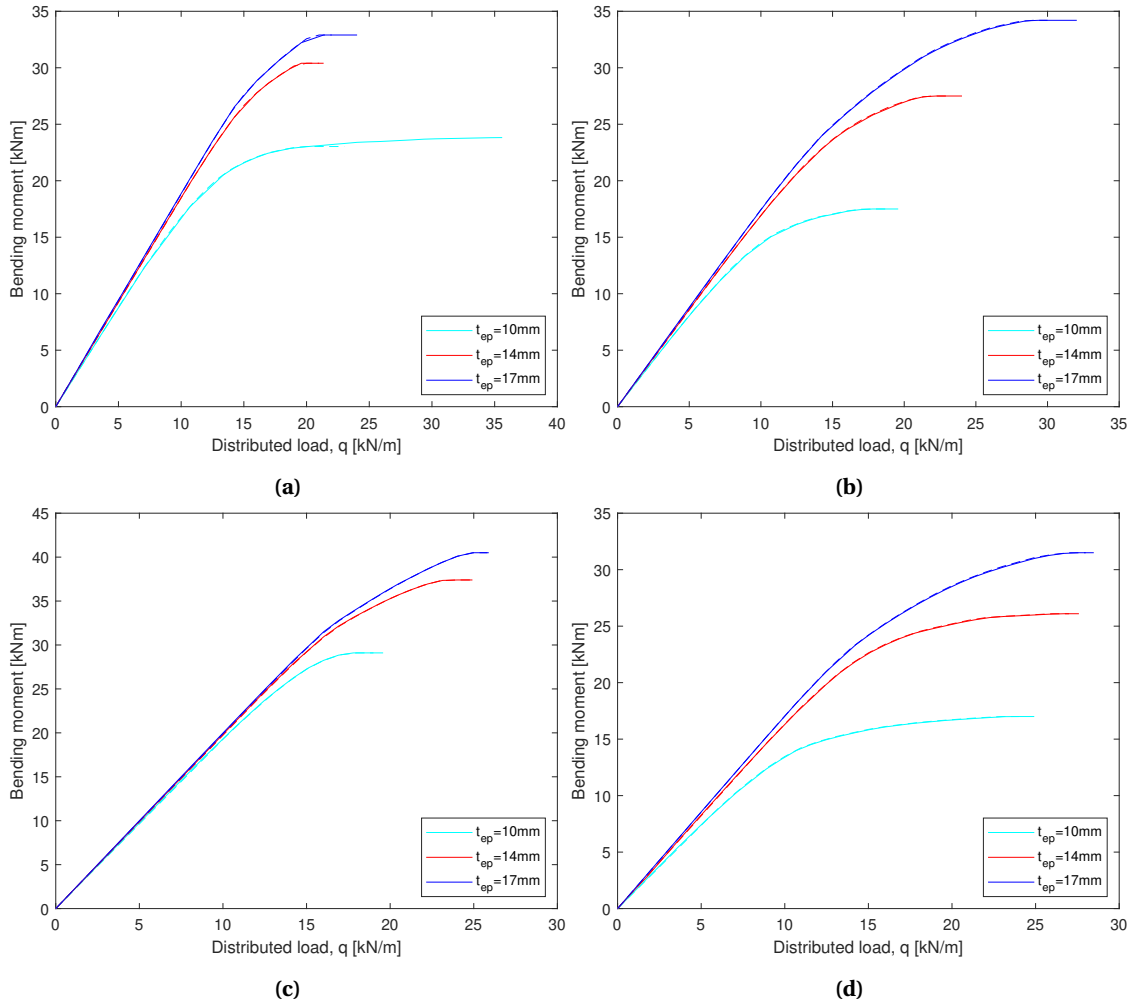

Figure 8.4: The bending moments at the joint as a function of q for (a) Model 1 (b) Model 2 (c) Model 3 (d) Model 4. The constant lines represents the numerical model and the dashed lines represents the analytical model.

The analytical and numerical method shows identical results of the bending moments due to both models using a linear-elastic material model. Figure 8.5 shows the numerical model using a non-linear material model.

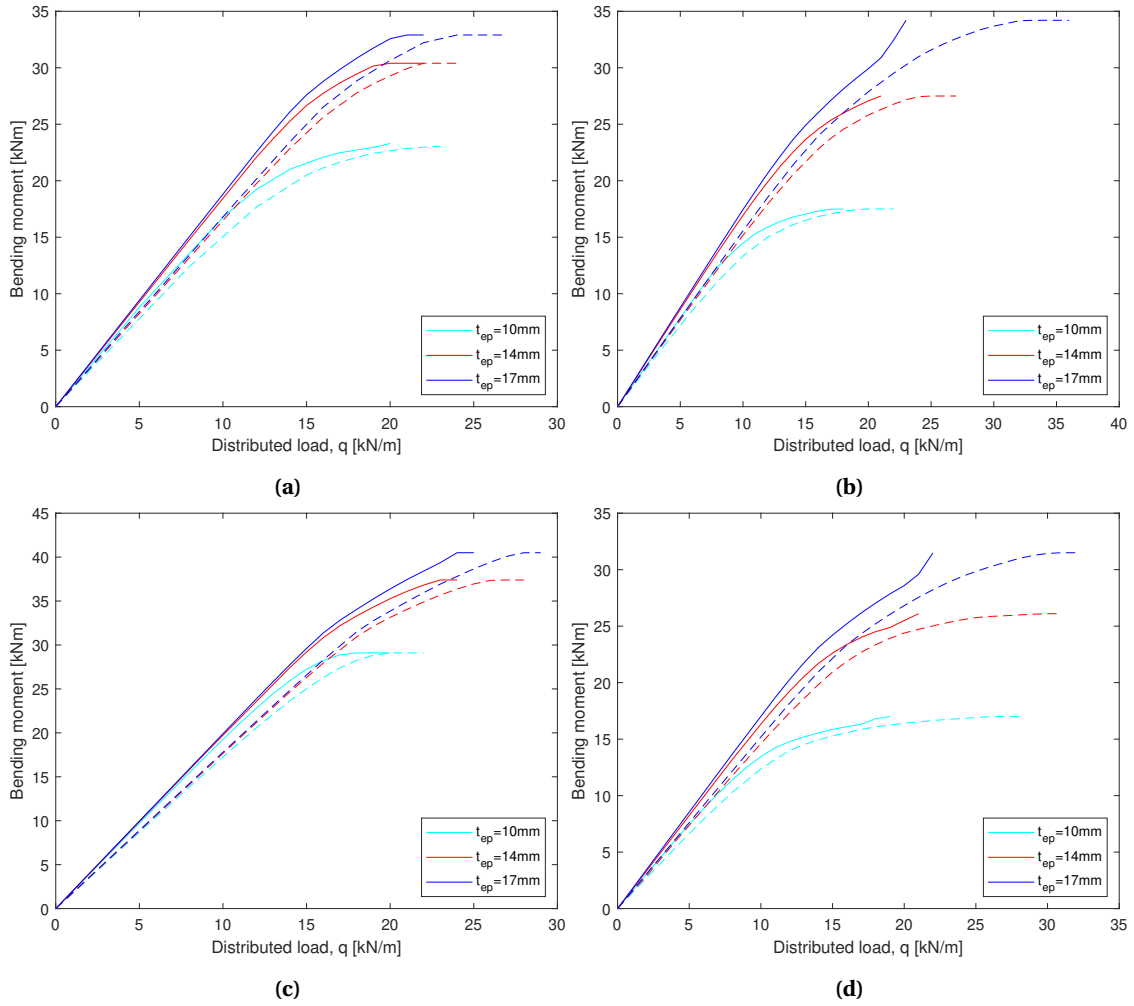

Figure 8.5: The bending moments at the joint for (a) Model 1 (b) Model 2 (c) Model 3 (d) Model 4. The constant lines represents the numerical model and the dashed lines represents the analytical model.

Using a non-linear material model for the numerical model the results deviates significantly in figure 8.5. The bending moment at the joint is greater for the numerical model at the same load compared to the analytical model.

The $M-\theta$-curve for both the analytical and numerical model determined in chapter 5.3 are compared in figure 8.6 with a material model which is elastic-perfectly plastic.

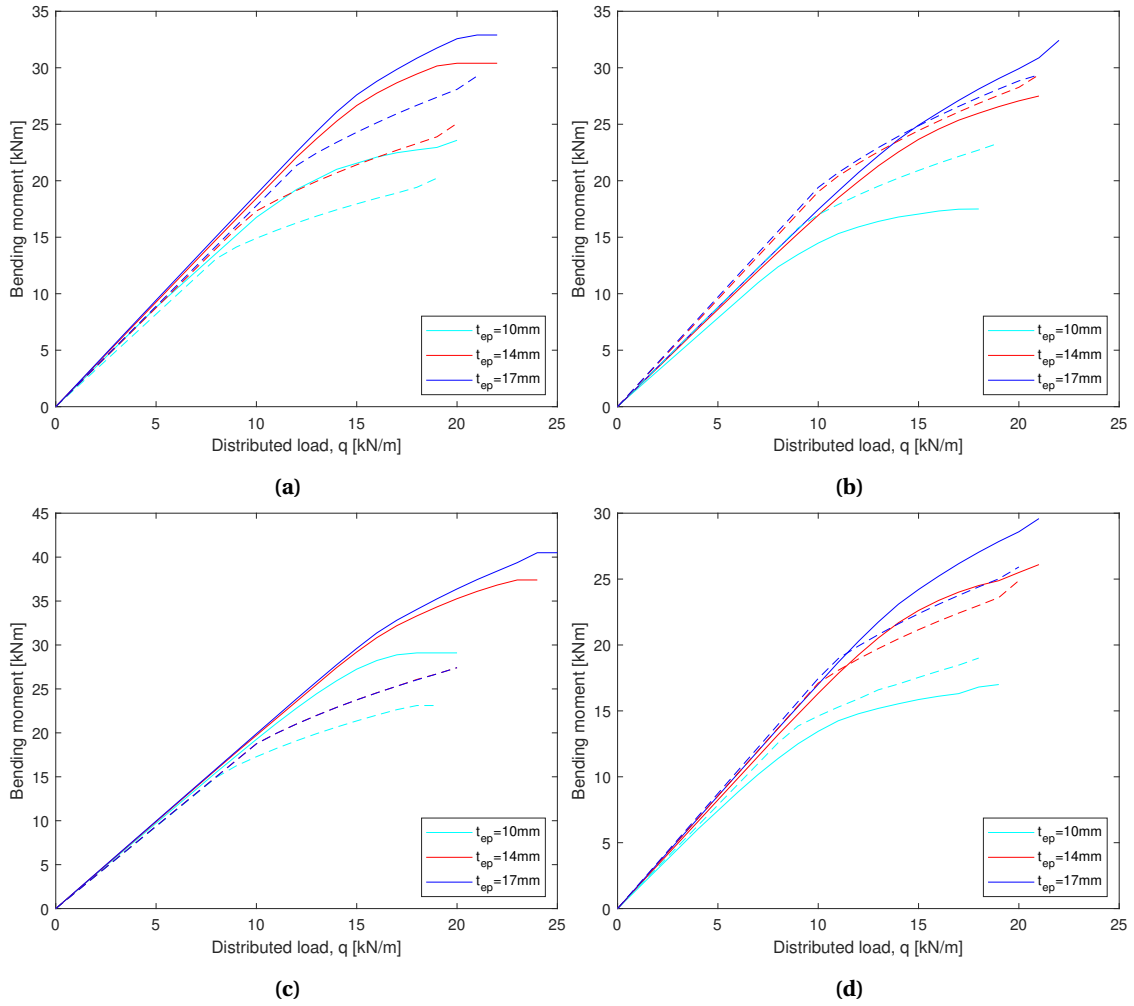

Figure 8.6: The bending moments at the joint for (a) Model 1 (b) Model 2 (c) Model 3 (d) Model 4. The constant lines represents the numerical model and the dashed lines represents the analytical model.

Figure 8.6 shows a great correlation between the bending moments in general at the linear part of the graph. When the bending moments reaches non-linearity it deviates significantly which also was showcased in chapter 5.3, when considering the moment-rotation curves. The figure also shows that the thinner end-plates reaches the non-linearity at a lower distributed load. The comparisons of the four models with the same end-plate thickness is shown in figure 8.7.

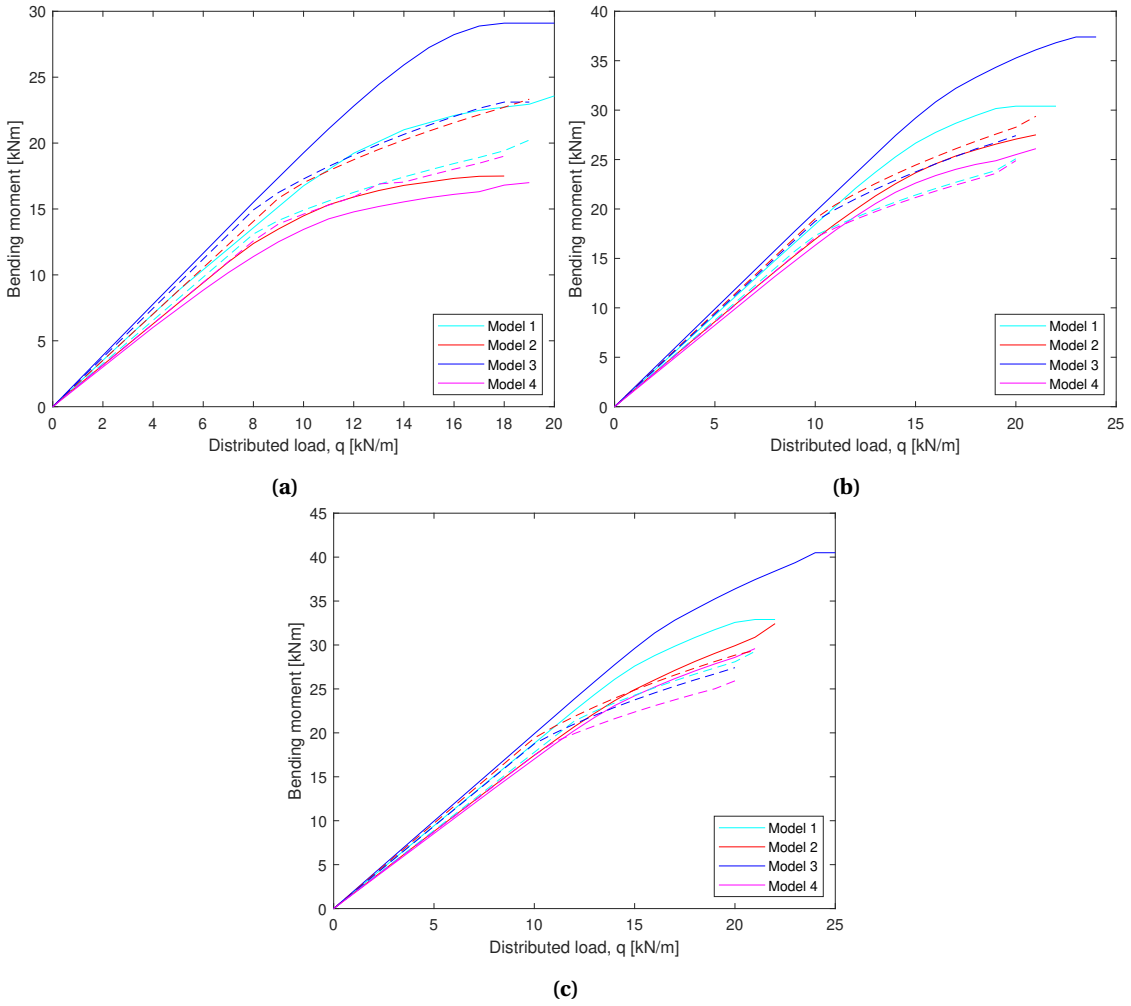

Figure 8.7: The bending moments at the joint for (a) end-plate thickness of 10 mm (b) end-plate thickness of 14 mm (c) end-plate thickness of 17 mm. The constant lines represents the numerical model and the dashed lines represents the analytical model.

Figure 8.7 shows that the joint of Model 3 attracts a greater bending moment when considering the distributed loads. This also aligns with the result obtained in chapter 5.3, as the stiffness of Model 3 is greater than the other models. The bending moment at the centre of the beam is also influenced by the linear distributed load, as is also indicated in figure 8.3. The bending moment at the middle of the beam is greater, when the joint tend towards a pinned connection. This can also illustrated using the obtained moment-rotation curve, see figure 8.8.

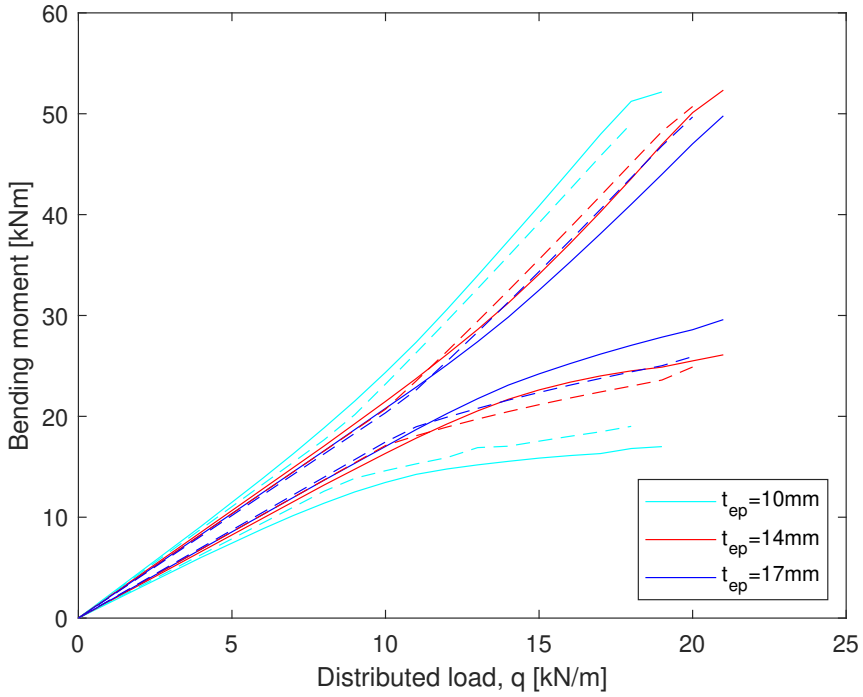

Figure 8.8: Comparison of the bending moment at the joint and the middle of the beam. The lower values are at the joint, while the greater values are at the middle of the beam

The comparison shown in figure 8.8 shows the increase in bending moments at the centre of the beam. When the bending moment at the joint reaches a plateau, the joint will resemble a pinned joint and the beam would then resemble a simple supported beam. Therefore the bending moments in the beam would increase at a greater rate, when the distributed load would increase.

IV

Closure

9. Conclusion and discussion

In this chapter the overall project is summarised and concluded upon. A general discussion of the two methods used is presented. The Models investigated are highlighted and compared.

Bolted joints are one of the most used methods of joining elements together in steel structures and buildings. Loads are transferred through the joints from one of the connected elements to the other. A bolted joint consists of a threaded bolt that joins two elements together secured by a nut. The assembly and structure of the joint as well as the steel grade used can influence the stiffness and moment bearing capacity. A portal frame with fixed supports are analysed and a vertical distributed force is applied to the beam. Steel grade S235 is used for the beam, column and end-plate while bolt grade M8.8 is used in the analysis. The design of the frame is not considered and therefore the design values evaluated is all the characteristics values. Four different joint configurations with different bolt-hole placements have been investigated, as well as the effects of varying end-plate thickness.

Two approaches to determining the effects of the joint configurations are used; the analytical method and numerical method. The analytical methods consists of the Component Method, to determine the moment bearing capacity and the other method is the slope-deflection method, to determine the effects the stiffness of the joint has on the bending moment distribution of the frame. The numerical method consists of the use of ANSYS to determine the moment bearing capacity and RFEM to investigate the influence the joint stiffness has on the bending moment diagram.

9.1 Moment bearing capacity

Firstly a convergence analysis has been performed for the numerical model, to determine if the number of elements used enough to gain an accurate result. A convergence analysis was conducted for the Model 1 of the joint in ANSYS. The result from the convergence analysis was used for the other models as well with the varying end-plate thickness.

The different models moment bearing capacity were used to investigate if the bolt placement had an influence in the analytical and numerical model. For the models with bolt placement at the edge of the end-plate ie. Model 2 and Model 3, the numerical model showed a decrease in the moment bearing capacity compared to the analytical model with an end-plate thickness of 10 mm. With an greater end-plate thickness the analytical and numerical method gave a larger moment bearing resistance which could indicate, that the end-plate thickness could be the limiting factor to a degree. With all the models with increasing end-plate thickness, the moment bearing resistance increased. The numerical models showcases an increase in moment bearing resistance, as it becomes greater than the analytical models when increasing the end-plate thickness. The reasoning could be the stress concentration around the bolt-holes, as the bolt-holes close to the edges cannot redistribute the stresses with a thin end-plate. Therefore with a thicker end-plate, the stresses around the bolt-holes redistributes better and the moment bearing capacity is therefore increased.

An issue of the Component Method is the complexity of the calculations. For a joint with one bolt-row in tension, the calculations is a bit more simple, as no bolt-row groups are considered. The complexity increases significantly with an increasing number of bolt-rows in tension. With two bolt-rows in tension, there is one group of bolt-rows which are considered, while three sets of bolt-row groups are considered for three bolt-rows in tension.

One problem that occurred in chapter 5 was that the simulations did not reach a moment plateau and aborted before it could. The reason for this could be the use of force control, and therefore the simulation could not reach a solution at a certain force. A different load scenario could have been used, for instance displacement control, but would have required a different model built as ANSYS cannot introduce a rotational deformation. Displacement control has its benefits as its typically more stable than load control, as an increase in displacement may not necessary increase the internal moments and forces. This in turn could lead to the simulations reaching a plateau where a larger deformation does not lead to an increase in bending moment. If displacement control should be used a larger model would need to be constructed, where half the frame is modelled, as symmetry then can be used. Although it can be discussed if a more precise result is beneficial as the computational time would increase significantly with a larger numerical model.

To determine the most precise and effective method to determine the moment bearing capacity involves a lot of factors. To determine the real behaviour of the investigated joints an experimental analysis should be conducted and could be used to calibrate the numerical model. The models used to determine the moment bearing capacity in the numerical method is a simplified model, which has not been compared to a full scale numerical model. The precision of the simplified model has not been checked and could vary significantly from a full scale numerical model.

9.2 Bending moment distribution

The different stiffness at the corners of the portal frame is investigated to determine how the joint stiffness influences the bending moment diagram of the frame. For the analytical method, with the slope-deflection method, one configuration is investigated where the beam and column centre-lines are connected. The numerical method is investigated in RFEM and two models are modelled. The first is where the centre-lines of the beam and columns are connected, and the second is where an eccentricity is introduced, at which the beam is connected to the flange of the column. The analytical method are assumed linear elastic while the numerical method is analysed using both a linear elastic and elastic-perfectly plastic material model. The bending moments are determined at the column foot, the joint between the column and beam, and the midpoint of the beam.

The two analysis methods showed identical bending moments at the investigated points if the linear elastic model where used and there were no eccentricity introduced in the numerical model. The analytical model and the numerical model with a joint eccentricity showed a small variation likely due to the different ways the models are constructed.

The non-linear moment-rotation curve determined from the moment bearing capacity is used to simulate the joints bending moment, when the frame is influenced by a linear distributed load. The load is increased gradually and shows the bending moments at the linear part are similar, but deviates when the joints reaches non-linearity, when the same model but with different end-plate thickness are compared.

References

ANSYS (2023a), *Connecting Bolts Represented as Beam Elements — Lesson 3*. Visited 25.11.2023. URL: https://courses.ansys.com/index.php/courses/connecting-bolts-with-the-rest-of-an-assembly/lessons/connecting-bolts-represented-as-beam-elements-lesson-3/.

— (2023b), *SHELL181*. Visited 08.11.2023. URL: https://www.mm.bme.hu/~gyebro/files/ans_help_v182/ans_elem/Hlp_E_SHELL181.html.

Augusto, Hugo et al. (2015), "Characterization of web panel components in double-extended bolted end-plate steel joints". In: *Journal of Constructional Steel Research*.

Cook, Robert et al. (2002), *Concepts and Application of Finite Element Analysis*. ISBN: 978-0-471-35605-9. University of Wisconsin.

Dansk Standard (2007), *Eurocode 3: Design of steel structures - Part 1-8 Design of joints*. Dansk Standard.

— (2022), *Eurocode 3: Design of steel structures - Part 1-1 General rules and rules for buildings*. Dansk Standard.

Dlubal (2022), *Finite Elements in RFEM*. Visited 15.11.2023. URL: https://www.dlubal.com/en/downloads-and-information/documents/online-manuals/rfem-6/000434.

— (2023a), *Analysis of Load-Bearing Capacity of Bolted Frame Joints According to EC 3-1-8*. Visited 23.01.24. URL: https://www.dlubal.com/en/support-and-learning/support/knowledge-base/001475.

— (2023b), *Member Eccentricities*. Visited 23.01.24. URL: https://www.dlubal.com/en/downloads-and-information/documents/online-manuals/rfem-6/000052.

Faella, Ciro et al. (1999), *Structural Steel Semirigid Connections: Theory, Design and software*. ISBN: 0-8493-7433-2. CRC Press LCC.

Golden Gate Bridge, Highway and Transportation District (2024), *Design & Construction Stats*. Visited 21.01.24. URL: https://www.goldengate.org/bridge/history-research/statistics-data/design-construction-stats/.

Henderson, Richard (2022), "Portal frames with flexible joints using Kleinlogel-type formulae". In: *NCS Technical Digest*.

Jaspart, Jean-Pierre and Klaus Weynand (2016), *Design of Joints in Steel and Composite Structures*. ECCS – European Convention for Constructional Steelwork.

Jensen, Bjarne Chr. et al. (2022), *Teknisk Ståbi*. 25. udgave ISBN: 978-87-571-2775-1. Nyt Teknisk Forlag.

Kleinlogel, Adolf (1953), *Rigid Frame Formulas*. ISBN: 0804445516. Wilhelm Ernst & Sohn.

Krenk, Steen (2009), *Non-linear Modeling and Analysis of Solids and Structures*. ISBN: 0521830540. Cambridge: Cambridge University Press.

McCormac, Jack C. and James K. Nelson (1997), *Structural Analysis: A Classical and Matrix Approach*. 2. edition ISBN: 0-673-99753-7. Addison Wesley.

Norris, Charles Head et al. (1997), *Elementary Structural Analysis*. 2. edition ISBN: 0-673-99753-7. Addison Wesley.

P., Jaspart J.- (2000), *Designing Structural Joints according to Eurocodes*. Kluwer Academic Publishers.

Unsplash (2018), *Golden Gate Bridge*. Visited 20.01.2024. URL: `https://unsplash.com/photos/san-francisco-bridge-usa-rX2cj2FD4do`.

Vayas, Ioannis et al. (2019), *Design of Steel Structures to Eurocodes*. Springer Tracts in Civil Engineering.

Weynand, Klaus et al. (1995), *The Stiffness Model of revised Annex J of Eurocode 3*. Elsevier Ltd.

Zoetemeijer, P. (1974), *A design method for the tension side of statically loaded, bolted beam-to-column connections*. HERON.

V

Appendix

A. Stiffness model of Eurocode 3

In this appendix the general model of the Component Method is presented which Annex J of Eurocode 3 provides.

A.1 Theory behind the Component Method

Annex J of Eurocode 3 provides the background of the Component Method. The annex also compares the Component Method with test results, which shows a good agreement between the two methods. The difference in resistance between the two methods is that the Component Method does not take strain hardening and membrane effects into account.

A.1.1 The general model

It is provided that the rotational capacity is not limited. In the general model of the component method consist of three parts. The first part is the linear elastic part up to 2/3 of the moment bearing resistance, $M_{j,rD}$. The corresponding stiffness is the initial stiffness, $S_{j,ini}$. After the first part, the curve becomes non-linear up until the moment reaches $M_{j,Rd}$ and it then will reach a yield plateau. This is illustrated in figure A.1.

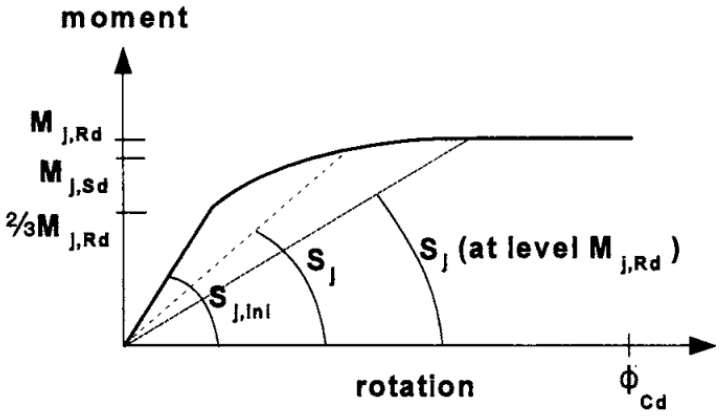

Figure A.1: The non-linaer $M-\theta$ curve.

The shape of the non-linear part is given with equation (A.1).

$$S_j = \frac{S_{j,ini}}{\left(\frac{1,5M_{j,Sd}}{M_{j,Rd}}\right)^{\psi}} \tag{A.1}$$

Where

ψ	for end-plated joint it is 2,7

It is then necessary to determine $S_{j,ini}$, to determine the stiffness of the non-linear part. The joint is considered as a spring, where the spring is connected to the intersection of the beam and column centrelines, see figure A.2. The properties of the spring expresses the relationship between the bending moment M_{Ed} and the corresponding rotation Φ_{Ed}.

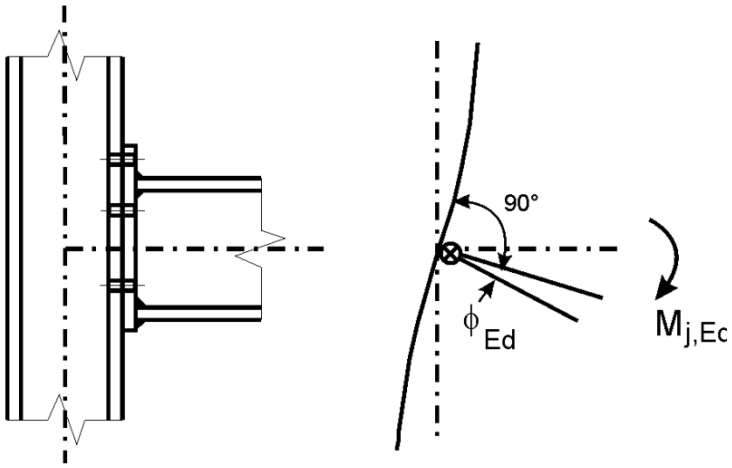

Figure A.2: The joint and how it is modelled.

The initial stiffness is derived from the elastic stiffness of the components, which can be represented as a rotational spring. The force-deformation relation is given by equation (A.2).

$$F_i = k_i \cdot E \cdot \Delta_i \tag{A.2}$$

Where

F_i	is the force in the spring of component i
k_i	is the stiffness coefficient of component i
E	is the Young modulus
Δ_i	is the spring deformation of component i

It can be observed in equation (A.2) that the stiffness of the the individual component is given as $k_i \cdot E$, which means the stiffness coefficients is a unit of length. Each of the components springs are combined into a single spring model, see figure A.3, which shows a spring model for a bolted end-plate with two bolt-rows in tension. From figure A.3 it can be seen that the moment M_j results in a rotation Φ_j. It is assumed that the deformation at the bolt-row is proportional to the distance to the centre of compression for all bolt-rows. Figure A.3 represents a spring model for an end-plated joint with two bolt-rows, where each spring has a stiffness coefficient of k_i.

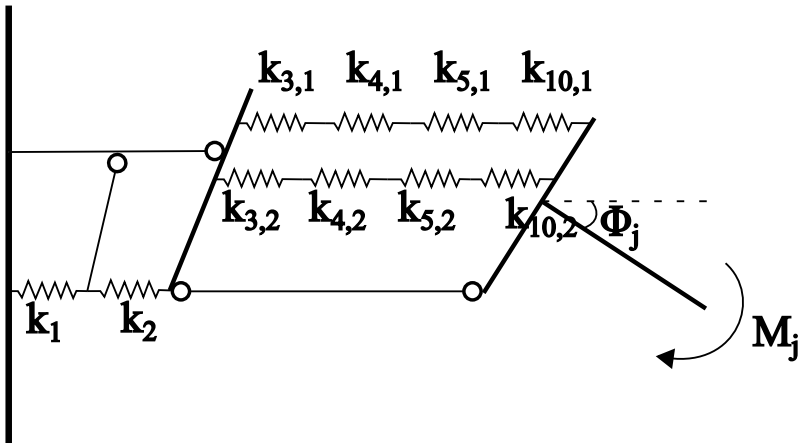

Figure A.3: The joint and how it is modelled.

Each spring represents a basic component, which is given as the following, where r indicates the bolt-row:

- k_1 - Column web panel in shear
- k_2 - Column web in compression
- $k_{3,r}$ - Column web in tension
- $k_{4,r}$ - Column flange in bending
- $k_{5,r}$ - End-plate in bending
- $k_{10,r}$ - Bolts in tension

The summarised force of all the springs in tension is equal til F. The moment M_j is then equal to $F\,z$, where z is the distance between the centre of tension and centre of compression. The rotation Φ_j can likewise be rewritten as equation (A.3).

$$\Phi_j = \frac{\sum \Delta_i}{z} \tag{A.3}$$

The initial stiffness can be derived from equation (A.2) and equation (A.3) and is given in equation (A.4).

$$S_{j,ini} = \frac{Ez^2}{\sum \frac{1}{k_i}} \tag{A.4}$$

With two bolt-rows the individuel stiffness coefficients can be substituted to an effective stiffness coefficient $k_{eff,r}$, representing the deformation for each bolt-row, and an equivalent stiffness coefficient k_{eq}, representing the total deformation for both bolt-rows, see figure A.4. The equivalent spring is acting with a lever arm z to the centre of compression. The equivalent stiffness k_{eq} can be used directly in equation (A.4).

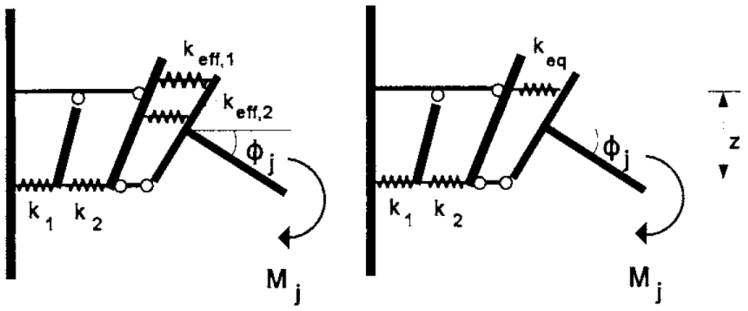

Figure A.4: The effective stiffness coefficient and equivalent stiffness coefficient.

To determine the stiffness coefficients, the concept of "equivalent T-stub" may be used. The method can both be used to calculate the strength and stiffness of the components. This is explained in chapter 4.1.

B. Worked Example - Component method

The joint stiffness and moment bearing capacity of Model 1 is determined in this worked example. The model consists of a HE240B column, an IPE200 beam, an end-plate with dimension 240 mm × 240 mm and 4 M16 bolts, see table B.1 for the dimensions. The worked example is based on Eurocode 3 Part 1-8.

	Parameter	**Unit**	**Value**
Beam IPE200	Height, h_b	mm	200
	Width, b_b	mm	100
	Thickness of the flange, t_{fb}	mm	8,5
	Thickness of the web, t_{wb}	mm	5,6
	Radius of root fillet, r_b	mm	12
	Moment of inertia, I_y	mm^4	$19,4\,10^6$
Column HE240B	Height, h_c	mm	240
	Width, b_c	mm	240
	Thickness of the flange, t_{fc}	mm	17
	Thickness of the web, t_{wc}	mm	10
	Radius of root fillet, r_c	mm	21
	Moment of inertia, I_y	mm^4	$80,9\,10^6$
End-plate	Height, h_{ep}	mm	240
	Width, b_{ep}	mm	240
	Thickness, t_{ep}	mm	10,14,17
Bolt M16	Diameter of shaft, d_i	mm	13,5
	Bolt-head height, h_b	mm	10
	Nut height, h_{nut}	mm	13
	Washer diameter, d_w	mm	30
	Washer thickness, t_w	mm	3
Steel	Yield strength, f_y	MPa	235
	Yield strength bolts, f_{yb}	MPa	640
	Modulus of elasticity, E	MPa	$2,1\,10^5$
	Poisson's ratio, ν		0,30

Table B.1: The dimensions used to determine the moment bearing capacity using the Component Method.

The placements of the beam and bolts are shown in figure B.1.

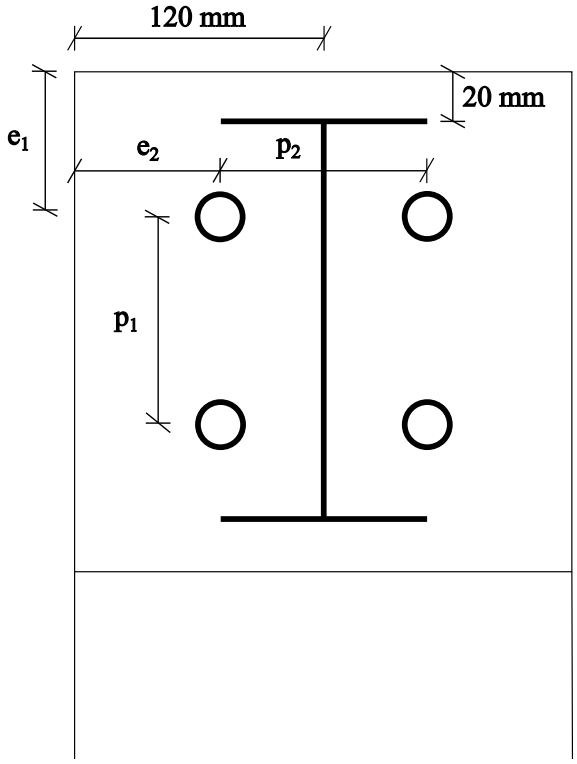

Figure B.1: The placements of the beam and bolts.

The four joint configurations are named Model 1-4 and described in table B.2.

	e_1 [mm]	e_2 [mm]	p_1 [mm]	p_2 [mm]
Model 1	70	70	100	100
Model 2	35	35	100	170
Model 3	45	70	100	100
Model 4	70	45	100	150

Table B.2: Description of the joint configuration.

B.1 Moment bearing resistance

The basic components are identified according to Eurocode 3 Part 1-8 as: *Column web in transverse tension, column flange in bending, end-plate in bending, beam web in tension and bolts in tension.* The procedure of determining the moment bearing resistance are divided into four steps:

- Step 1 - Identify the key dimensions to determine l_{eff}
- Step 2 - Calculate l_{eff}
- Step 3 - Calculate the resistance of the T-stubs and web panels
- Step 4 - Determine the moment bearing capacity

B.1.1 Step 1

Step 1 is to identify the key elements to determine l_{eff} for the column flange and end-plate.

Column flange in bending

Clause 6.2.6.4 in Eurocode 3 Part 1-8.

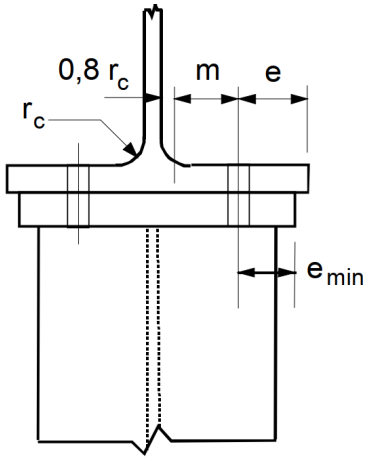

Figure B.2: The dimensions of m, r_c, e and e_{min} where $e = e_{min} = e_2$.

Due to the end-plate and column flange having the same width, $e = e_{min} = e_2$. m is determined for the column:

$$m_c = \frac{p_2}{2} - \frac{t_{wc}}{2} - 0,8r_c = \frac{100\text{mm}}{2} - \frac{10\text{mm}}{2} - 0,8 \cdot 21\text{mm}$$
$$m_c = 28,2\text{mm}$$

End-plate in bending

Clause 6.2.6.5 in Eurocode 3 Part 1-8.

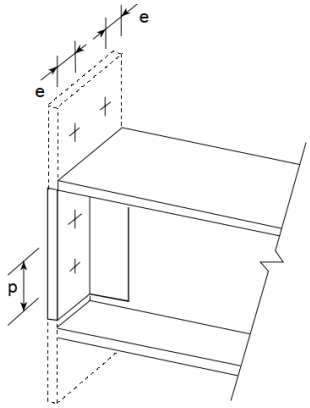

Figure B.3: The dimensions of e and p where $p = p_1$.

m is determined for the end-plate:

$$m_{ep} = \frac{p_1}{2} - \frac{t_{wb}}{2} - 0,8r_c = \frac{100\text{mm}}{2} - \frac{5,6\text{mm}}{2} - 0,8 \cdot 12\text{mm}$$
$$m_{ep} = 37,60\text{mm}$$

The beam flange is considered a stiffener and therefor the α value is determined. m_2 is shown in figure B.4.

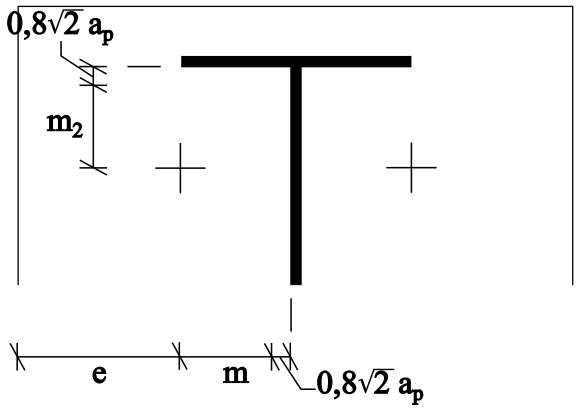

Figure B.4: The values of m and m_2. a_p is the length of the weld root

$$\lambda_1 = \frac{m_{ep}}{m_{ep} + e} = \frac{37,6\text{mm}}{37,6\text{mm} + 70\text{mm}}$$
$$\lambda_1 = 0,35$$
$$\lambda_2 = \frac{m_2}{m_{ep} + e} = \frac{43,6\text{mm}}{37,6\text{mm} + 70\text{mm}}$$
$$\lambda_2 = 0,41$$
$$\alpha = 6,5$$

α is read on graph from Eurocode 3 Part 1-8 figure 6.11.

B.1.2 Step 2

Step 2 is to determine the effective lengths for the column flange in bending and end-plate in bending. The effective length are determined for bolt-row 1, 2 and as a bolt-row group and are denoted as follows for mode 1 for the column flange in bending:

$l_{eff,1,fc,1}$	Effective length for bolt-row 1 at mode 1
$l_{eff,1,fc,2}$	Effective length for bolt-row 2 at mode 1
$l_{eff,1,fc,1-2}$	Effective length for bolt-row group at mode 1

The effective length for the end-plate in bending will have the subscript "ep".

Column flange in bending

Bolt-row location: Bolt-row 1, 2 and group

Bolt-row 1:

$$l_{eff,cp,1} = \min\left(\begin{bmatrix} 2\pi m_c \\ \pi m_c + 2e_1 \end{bmatrix}\right) = \min\left(\begin{bmatrix} 2\pi \cdot 28,2\text{mm} \\ \pi \cdot 28,2\text{mm} + 2 \cdot 70\text{mm} \end{bmatrix}\right)$$

$$l_{eff,cp,1} = 177,19\text{mm}$$

$$l_{eff,nc,1} = \min\left(\begin{bmatrix} 4m_c + 1,25e \\ 2m_c + 0,625e + e_1 \end{bmatrix}\right) = \min\left(\begin{bmatrix} 4 \cdot 28,2\text{mm} + 1,25 \cdot 70\text{mm} \\ 2 \cdot 28,2\text{mm} + 0,625 \cdot 70\text{mm} + 70\text{mm} \end{bmatrix}\right)$$

$$l_{eff,nc,1} = 170,15\text{mm}$$

Bolt-row 2:

$$l_{eff,cp,2} = 2\pi m_c = 2\pi \cdot 28,2\text{mm}$$

$$l_{eff,nc,1} = 177,19\text{mm}$$

$$l_{eff,nc,2} = 4m_c + 1,25e = 4 \cdot 28,2\text{mm} + 1,25 \cdot 70\text{mm}$$

$$l_{eff,nc,2} = 200,30\text{mm}$$

Bolt-row 1 as a group:

$$l_{eff,cp,gr1} = \min\left(\begin{bmatrix} \pi m_c + p_1 \\ 2e_1 + p_1 \end{bmatrix}\right) = \min\left(\begin{bmatrix} \pi \cdot 28,2\text{mm} + 100\text{mm} \\ 2 \cdot 70\text{mm} + 100\text{mm} \end{bmatrix}\right)$$

$$l_{eff,cp,gr1} = 188,59\text{mm}$$

$$l_{eff,nc,gr1} = \min\left(\begin{bmatrix} 2m_c + 0,625e + 0,5p_1 \\ e_1 + 0,5p_1 \end{bmatrix}\right)$$

$$= \min\left(\begin{bmatrix} 2 \cdot 28,2\text{mm} + 0,625 \cdot 70\text{mm} + 0,5 \cdot 100\text{mm} \\ 100\text{mm} + 0,5 \cdot 100\text{mm} \end{bmatrix}\right)$$

$$l_{eff,nc,gr1} = 120,00\text{mm}$$

Bolt-row 2 as a group:

$$l_{eff,cp,gr2} = \min\left(\begin{bmatrix} \pi m_c + p_1 \\ 2e_1 + p_1 \end{bmatrix}\right) = \min\left(\begin{bmatrix} \pi \cdot 28,2\text{mm} + 100\text{mm} \\ 2 \cdot 70\text{mm} + 100\text{mm} \end{bmatrix}\right)$$

$$l_{eff,cp,gr2} = 177,19\text{mm}$$

$$l_{eff,nc,gr2} = \min\left(\begin{bmatrix} 2m_c + 0,625e + 0,5p_1 \\ e_1 + 0,5p_1 \end{bmatrix}\right)$$

$$= \min\left(\begin{bmatrix} 2 \cdot 28,2\text{mm} + 0,625 \cdot (70\text{mm} + 100\text{mm}) + 0,5 \cdot 100\text{mm} \\ 70\text{mm} + 100\text{mm} + 0,5 \cdot 100\text{mm} \end{bmatrix}\right)$$

$$l_{eff,nc,gr2} = 150,15\text{mm}$$

The effective length for the individual bolt-rows for mode 1 and 2 is determined with the following equations:

Mode 1

$$l_{eff,1} = \min\left(\begin{bmatrix} l_{eff,cp} \\ l_{eff,nc} \end{bmatrix}\right)$$

Mode 2

$$l_{eff,2} = l_{eff,nc}$$

The effective length for the a bolt-row group for mode 1 and 2 is determined with the following equations:

Mode 1

$$\sum l_{eff,1} = \min\left(\begin{bmatrix} \sum l_{eff,cp} \\ \sum l_{eff,nc} \end{bmatrix}\right)$$

Mode 2

$$\sum l_{eff,2} = \sum l_{eff,nc}$$

The effective lengths becomes for individual bolt-rows:

Mode 1

$l_{eff,1,fc,1} = 170,15\text{mm}$

$l_{eff,1,fc,2} = 177,19\text{mm}$

$l_{eff,1,fc,1-2} = 270,15\text{mm}$

Mode 2

$l_{eff,2,fc,1} = 170,15\text{mm}$

$l_{eff,2,fc,2} = 200,30\text{mm}$

$l_{eff,2,fc,1-2} = 270,15\text{mm}$

End-plate in bending

The same procedure is done with the end-plate with the use of different expressions for l_{eff} which is from Eurocode 3 Part 1-8 Table 6.6.

Bolt-row 1:

$l_{eff,cp,1} = 2\pi m_{ep} = 2\pi \cdot 37,6\text{mm}$

$l_{eff,cp,1} = 236,25\text{mm}$

$l_{eff,nc,1} = \alpha m_{ep} = 6,5 \cdot 37,6\text{mm}$

$l_{eff,nc,1} = 244,40\text{mm}$

Bolt-row 2:

$l_{eff,cp,2} = 2\pi m_{ep} = 2\pi \cdot 37,6\text{mm}$

$l_{eff,cp,2} = 236,25\text{mm}$

$l_{eff,nc,2} = 4m_{ep} + 1,25e_1 = 4 \cdot 37,6\text{mm} + 1,25 \cdot 70\text{mm}$

$l_{eff,nc,2} = 237,90\text{mm}$

Bolt-row 1 as a group:

$l_{eff,cp,gr1} = \pi m_{ep} + p_1 = \pi \cdot 37,6\text{mm} + 100\text{mm}$

$l_{eff,cp,gr1} = 218,12\text{mm}$

$l_{eff,nc,gr1} = 0,5p + \alpha m_{ep} - (2m_{ep} + 0,625e_1)$

$= 0,5 \cdot 100\text{mm} + 6,5 \cdot 37,6\text{mm} - (2 \cdot 37,6\text{mm} + 0,625 \cdot 70\text{mm})$

$l_{eff,nc,gr1} = 175,45\text{mm}$

Bolt-row 2 as a group:

$l_{eff,cp,gr2} = \pi m_{ep} + p = \pi \cdot 37,6\text{mm} + 100\text{mm}$

$l_{eff,cp,gr2} = 218,12\text{mm}$

$l_{eff,nc,gr2} = 2m_{ep} + 0,625e_1 + 0,5p = 2 \cdot 37,6\text{mm} + 0,625 \cdot 70\text{mm} + 0,5 \cdot 100\text{mm}$

$l_{eff,nc,gr2} = 168,95\text{mm}$

The effective lengths becomes for individual bolt-rows:

Mode 1

$l_{eff,1,ep,1} = 236,25\text{mm}$

$l_{eff,1,ep,2} = 236,25\text{mm}$

$l_{eff,1,ep,1-2} = 344,40\text{mm}$

Mode 2

$l_{eff,2,ep,1} = 244,40\text{mm}$

$l_{eff,2,ep,2} = 237,90\text{mm}$

$l_{eff,2,ep,1-2} = 344,40\text{mm}$

B.1.3 Step 3

Step 3 is to determine the resistance of the T-stub and web panels.

Column flange in bending

First it is checked if prying forces develops. Prying forces develops if the following condition applies:

$$L_b \leq L_b^* = \frac{8,8 m_c^3 A_s}{l_{eff,1,fc} t_{fc}^3}$$

A_s is the shear area of the bolt and is 157mm^2. L_b is the bolts elongation length and is equal to 46 mm and $m_c = 28,2$mm and $t_{fc} = 17$mm. L_b^* is determined for bolt-row 1, 2 and the bolt group.

$$l_{eff,1,fc,1} = 170,15\text{mm}$$
$$l_{eff,1,fc,2} = 177,19\text{mm}$$
$$l_{eff,1,fc,1-2} = 270,15\text{mm}$$
$$L_b = 46\text{mm} \not\leq L_b^* = \left(\begin{bmatrix} 37,06\text{mm} \\ 35,59\text{mm} \\ 23,34\text{mm} \end{bmatrix} \right)$$

Prying forces does not develop in this joint configuration and therefore only $M_{pl,1}$ is used. In case prying forces develops both $M_{pl,1}$ and $M_{pl,2}$ needs to be determined. The plastic bending resistance can be determined for bolt-row 1, 2 and the bolt group with the known effective lengths and then the tension resistance is determined afterwards.

The tension resistance for the column flange in bending can now be determined. The effective lengths are calculated earlier and given as:

Mode 1

$$l_{eff,1,fc,1} = 170,15\text{mm}$$
$$l_{eff,1,fc,2} = 177,19\text{mm}$$
$$l_{eff,1,fc,1-2} = 270,15\text{mm}$$

Mode 2

$$l_{eff,2,fc,1} = 170,15\text{mm}$$
$$l_{eff,2,fc,2} = 200,30\text{mm}$$
$$l_{eff,2,fc,1-2} = 270,15\text{mm}$$

Tension resistance Mode 1 and 2 for the column flange in bending:

The column flange thickness is given as 17 mm and $f_y = 235$ MPa.

$$M_{pl,1,fc} = 0,25 \cdot l_{eff,1,fc} t_{fc}^2 f_y = 0,25 l_{eff,1,fc} \cdot (17\text{mm})^2 \cdot 235\text{MPa}$$
$$M_{pl,1,fc} = \left(\begin{bmatrix} 2,89\text{kNm} \\ 3,01\text{kNm} \\ 4,59\text{kNm} \end{bmatrix} \right)$$

$$F_{T,1-2,fc} = \frac{2M_{pl,1,fc}}{m_c} = \frac{2M_{pl,1,fc}}{28,2\text{mm}}$$
$$F_{T,1-2,fc} = \left(\begin{bmatrix} 204,89\text{kN} \\ 213,36\text{kN} \\ 325,31\text{kN} \end{bmatrix} \right)$$

Tension resistance Mode 3 for the column flange in bending:

Mode 3 is bolt failure and is given as:

$$F_{T,3,fc} = \sum (n_b F_t)$$

n_b is the number of bolts in one bolt-row, which is 2 bolts. F_t is the tension resistance of a single bolt. k_2 is given as 0,9 according to Eurocode 3 Part 1-8.

$$F_t = k_2 f_{yb} A_s = 0,9 \cdot 235\text{MPa} \cdot 157\text{mm}^2$$
$$F_t = 90,43\text{kN}$$

The bolt resistance for each bolt-row:

$$F_{T,3,fc} = \left(\begin{bmatrix} 180,86\text{kN} \\ 180,86\text{kN} \\ 361,72\text{kN} \end{bmatrix} \right)$$

End-plate in bending

The same procedure is repeated to determine the tension resistance of the end-plate. First it is checked if prying forces develops, where L_b, A_s is the same as before and $m_{ep} = 34,6$mm. The end-plate thickness is 10 mm:

$l_{eff,1,ep,1} = 236,25\text{mm}$

$l_{eff,1,ep,2} = 236,25\text{mm}$

$l_{eff,1,ep,1-2} = 344,40\text{mm}$

$$L_b \leq L_b^* = \frac{8,8 m_{ep}^3 A_s}{l_{eff,1,ep} t_{ep}^3}$$

$$L_b = 46 \leq L_b^* = \left(\begin{bmatrix} 310,87\text{mm} \\ 310,87\text{mm} \\ 213,25\text{mm} \end{bmatrix} \right)$$

Prying forces develops. The tension resistance for end-plate in bending can now be determined. The effective lengths for the end-plate is given as:

Mode 1

$l_{eff,1,ep,1} = 236,25\text{mm}$

$l_{eff,1,ep,2} = 236,25\text{mm}$

$l_{eff,1,ep,1-2} = 344,40\text{mm}$

Mode 2

$l_{eff,2,ep,1} = 244,40\text{mm}$

$l_{eff,2,ep,2} = 237,90\text{mm}$

$l_{eff,2,ep,1-2} = 344,40\text{mm}$

Tension resistance Mode 1 for the end-plate in bending:

Method 1:

$$M_{pl,1,ep} = 0,25 l_{eff,1,ep} t_p^2 f_y = 0,25 \cdot l_{eff,1,ep} \cdot (10\text{mm})^2 \cdot 235\text{MPa}$$

$$M_{pl,1,ep} = \left(\begin{bmatrix} 1,39\text{kNm} \\ 1,39\text{kNm} \\ 2,02\text{kNm} \end{bmatrix} \right)$$

$$F_{T,1,method1,ep} = \frac{4M_{pl,1,ep}}{m_{ep}} = \frac{4M_{pl,1,ep}}{37,6\text{mm}}$$

$$F_{T,1,method1,ep} = \left(\begin{bmatrix} 147,65\text{kN} \\ 147,65\text{kN} \\ 215,25\text{kN} \end{bmatrix} \right)$$

Method 2:

$$n_{ep} = \min\left(\begin{bmatrix} e_{min} \\ 1,25 m_{ep} \end{bmatrix} \right) = \min\left(\begin{bmatrix} 70\text{mm} \\ 1,25 \cdot 37,6\text{mm} \end{bmatrix} \right)$$

$$n_{ep} = 47\text{mm}$$

$$e_w = \frac{d_w}{4} = \frac{30\text{mm}}{4}$$

$$e_w = 7,5\text{mm}$$

$$F_{T,1,method2,ep} = \frac{(8n_{ep} - 2e_w) M_{pl,1,ep}}{2m_{ep}n_{ep} - e_w(m_{ep} + n_{ep})} = \frac{(8 \cdot 47\text{mm} - 2 \cdot 7,5\text{mm}) M_{pl,1,ep}}{2 \cdot 37,6\text{mm} \cdot 47\text{mm} - 7,5\text{mm} \cdot (37,6\text{mm} + 47\text{mm})}$$

$$F_{T,1,method2,ep} = \left(\begin{bmatrix} 172,78\text{kN} \\ 172,78\text{kN} \\ 251,88\text{kN} \end{bmatrix} \right)$$

Tension resistance Mode 2 for the end-plate in bending:

$$M_{pl,2,ep} = 0,25 l_{eff,2,ep} t_{ep}^2 f_y = 0,25 \cdot l_{eff,2,ep} \cdot (10\text{mm})^2 \cdot 235\text{MPa}$$

$$M_{pl,2,ep} = \left(\begin{bmatrix} 1,44\text{kNm} \\ 1,40\text{kNm} \\ 2,02\text{kNm} \end{bmatrix} \right)$$

$$F_{T,2,ep} = \frac{2M_{pl,2,ep} + n_{ep} \sum F_t}{m_{ep} + n_{ep}} = \frac{2M_{pl,2,ep} + 47\text{mm} \sum F_t}{37,6\text{mm} + 47\text{mm}}$$

$$F_{T,2,ep} = \left(\begin{bmatrix} 134,42\text{kN} \\ 133,52\text{kN} \\ 148,31\text{kN} \end{bmatrix} \right)$$

Tension resistance Mode 3 for the end-plate in bending:

The tensions resistance of the bolts are the same as the one calculated for column flange in bending.

$$F_{T,3,ep} = \left(\begin{bmatrix} 180,86\text{kN} \\ 180,86\text{kN} \\ 361,72\text{kN} \end{bmatrix} \right)$$

Column web in transverse tension

The effective width $b_{eff,t,wc}$ is taken equal to $l_{eff,1,fc}$ due to being lower than $l_{eff,2,fc}$. The shear area A_{vc} of the column web is determined as well as the reduction factor ω.

$$b_{eff,t,wc,1} = 170,15\text{mm}$$
$$b_{eff,t,wc,2} = 177,19\text{mm}$$
$$b_{eff,t,wc,1-2} = 270,15\text{mm}$$
$$A_{vc} = \max\left(\begin{bmatrix} A_c - 2b_c t_{fc} + (t_{wc} 2r_c) t_{fc} \\ \eta h_{wc} t_{wc} \end{bmatrix} \right)$$
$$= \max\left(\begin{bmatrix} 10,6 \cdot 10^3\text{mm}^2 - 2 \cdot 240\text{mm} \cdot 17\text{mm} + (10\text{mm} \cdot 2 \cdot 21\text{mm}) \cdot 17\text{mm} \\ 1,0 \cdot 206\text{mm} \cdot 10\text{mm} \end{bmatrix} \right)$$
$$A_{vc} = 3324\text{mm}^2$$
$$\omega = \frac{1}{1 + 1,3\left(b_{eff,t,wc} \frac{t_{wc}}{A_{vc}} \right)^2} = \frac{1}{1 + 1,3\left(b_{eff,t,wc} \frac{10\text{mm}}{3324\text{mm}^2} \right)^2}$$
$$\omega = \left(\begin{bmatrix} 0,75 \\ 0,73 \\ 0,54 \end{bmatrix} \right)$$

From the given values, the tension resistance for the column web in transverse tension is given as:

$$F_{t,wc} = \omega b_{eff,t,wc} t_{wc} f_y = b_{eff,t,wc} \cdot 10\text{mm} \cdot 235\text{MPa}$$
$$F_{t,wc} = \left(\begin{bmatrix} 298,26\text{kN} \\ 304,07\text{kN} \\ 341,56\text{kN} \end{bmatrix} \right)$$

Beam web in tension

The effective width $b_{eff,t,wb}$ is taken equal to $l_{eff,1,ep}$ due to being lower than $l_{eff,2,ep}$.

$$b_{eff,t,wb,1} = 236,25\text{mm}$$
$$b_{eff,t,wb,2} = 236,25\text{mm}$$
$$b_{eff,t,wb,1-2} = 344,40\text{mm}$$
$$F_{t,wb} = b_{eff,t,wb} t_{wb} f_y = b_{eff,t,wb} \cdot 5,6\text{mm} \cdot 235\text{MPa}$$
$$= F_{t,wb} \left(\begin{bmatrix} 310,90\text{kN} \\ 310,90\text{kN} \\ 453,23\text{kN} \end{bmatrix} \right)$$

Column web in compression

The effective width is determined. $\sqrt{2}a_p$ is the leg-size of the weld and is 8 mm. s is equal to $r_c = 27$ mm. s_p is equal to t_{ep} and is the length when dispersing through the end-plate at a 45° angle.

$$b_{eff,c,wc} = t_{fb} + 2\sqrt{2}a_p + 5(t_{fc} + s) + s_p$$
$$= 8,5\text{mm} + 2 \cdot 8\text{mm} + 5 \cdot (17\text{mm} + 27\text{mm}) + 10\text{mm} = 216,5\text{mm}$$

ρ is determined from the plate slenderness $\bar{\lambda}_p$. d_{wc} is the web panel depth and is given as 164 mm

$$\bar{\lambda}_p = 0,932\sqrt{\frac{b_{eff,c,wc} d_{wc} f_y}{E t_{wc}^2}} = 0,932\sqrt{\frac{216,5\text{mm} \cdot 164\text{mm} \cdot 235\text{MPa}}{210000\text{MPa} \cdot (10\text{mm})^2}}$$
$$\bar{\lambda}_p = 0,58 \quad \Rightarrow \quad \rho = 1$$

ω is determined:

$$\omega = \frac{1}{1 + 1,3\left(b_{eff,c,wc}\frac{t_{wc}}{A_{vc}}\right)^2} = \frac{1}{1 + 1,3 \cdot \left(216,5\text{mm} \cdot \frac{10\text{mm}}{3324\text{mm}}\right)^2}$$
$$\omega = 0,64$$

The resistance of the column web in compression is determined where $k_{wc} = 1$.

$$F_{c,wc} = \min\left(\begin{bmatrix} \omega k_{wc} b_{eff,c,wc} t_{wc} f_y \\ \omega k_{wc} \rho b_{eff,c,wc} t_{wc} f_y \end{bmatrix} \right) = \min\left(\begin{bmatrix} 0,64 \cdot 1 \cdot 216,5\text{mm} \cdot 10\text{mm} \cdot 235\text{MPa} \\ 0,64 \cdot 1 \cdot 1 \cdot 216,5\text{mm} \cdot 10\text{mm} \cdot 235\text{MPa} \end{bmatrix} \right)$$
$$F_{c,wc} = 325,62\text{kN}$$

Web panel in shear

The resistance of the web panel in shear is determined. The shear are of the column was claculated earlier to 3324mm^2.

$$V_{wp} = \frac{0,9 f_y A_{vc}}{\sqrt{3}} = \frac{0,9 \cdot 235\text{MPa} \cdot 3325\text{mm}^2}{\sqrt{3}}$$
$$V_{wp} = 405,89\text{kN}$$

Summary: Resistance of the T-stub

The resistance for the individual T-stubs is the lowest resistence for each bolt-row and the group of bolt-rows and is given as follows:

$$F_T = \left(\begin{bmatrix} 134,42\text{kN} \\ 133,52\text{kN} \\ 148,31\text{kN} \end{bmatrix} \right)$$

The sum of the tension resistance of the first two rows are greater than the tension resistance for the bolt-row groups. The individual bolt-row tension resistance needs to satisfy the following:

$$F_{T,r1} + F_{T,r2} \leq F_{T,r1-2}$$

The tension resistance of the individual bolt-row is reduced so it satisfies the expression. The tension resistance of the bolt-row at the bottom is reduced until it is satisfied and therefore becomes:

$$F_T = \left(\begin{bmatrix} 134,42\text{kN} \\ 13,89\text{kN} \\ 148,31\text{kN} \end{bmatrix} \right)$$

B.1.4 Step 4

The last step is to determine the moment bearing capacity. The moment bearing capacity is determined as the following:

$$M_j = \sum_r h_r F_{tr} = 145,75\text{mm} \cdot 134,42\text{kN} + 45,75\text{mm} \cdot 13,89\text{kN}$$
$$M_j = 20,23\text{kNm}$$

B.2 Rotational stiffness

The individual components stiffness coefficients is determined for row 1 and 2. z is taken as the midway point between the two bolt-rows to the centre of compression and is 95,75 mm:

$$k_1 = \frac{0,38A_{vc}}{\beta z} = \frac{0,38 \cdot 3324\text{mm}^2}{1 \cdot 95,75\text{mm}}$$

$$k_1 = 13,19\text{mm}$$

$$k_2 = \frac{0,7b_{eff,c,wc}t_{wc}}{d_c} = \frac{0,7 \cdot 216,5\text{mm} \cdot 10\text{mm}}{164\text{mm}}$$

$$k_2 = 9,10\text{mm}$$

$$k_{3,r} = \frac{0,7b_{eff,t,wc,r}t_{wc}}{d_c} = \frac{0,7 \cdot b_{eff,t,wc}10\text{mm}}{164\text{mm}}$$

$$k_{3,r} = \left(\begin{bmatrix} 7,26\text{mm} \\ 7,56\text{mm} \end{bmatrix} \right)$$

$$k_{4,r} = \frac{0,9l_{eff,fc,r}t_{fc}^3}{d_c^3} = \frac{0,91 \cdot l_{eff,fc,r} \cdot (17\text{mm})^3}{(164\text{mm})^3}$$

$$k_{4,r} = \left(\begin{bmatrix} 23,66\text{mm} \\ 29,61\text{mm} \end{bmatrix} \right)$$

$$k_{5,r} = \frac{0,9l_{eff,ep,r}t_p^3}{m_{ep}^3} = \frac{0,9 \cdot l_{eff,ep,r} \cdot (10\text{mm})^3}{(37,6\text{mm})^3}$$

$$k_{5,r} = \left(\begin{bmatrix} 2,97\text{mm} \\ 2,86\text{mm} \end{bmatrix} \right)$$

$$k_{10} = \frac{1,6A_s}{L_b} = \frac{1,6 \cdot 157\text{mm}}{46\text{mm}}$$

$$= k_{10} = 5,46\text{mm}$$

k_{eff} is determined where $k_{3,r}$, $k_{4,r}$, $k_{5,r}$ and k_{10} is used for each bolt-row.

$$k_{eff,r} = \frac{1}{\sum_i \frac{1}{k_{i,r}}} = \left(\begin{bmatrix} 1,43\text{mm} \\ 1,43\text{mm} \end{bmatrix} \right)$$

z_{eq} and k_{eq} is determined:

$$z_{eq} = \frac{\sum_r k_{eff,r} h_r^2}{\sum_r k_{eff,r} h_r} = \frac{1,43\text{mm} \cdot (145,75\text{mm})^2 + 1,43\text{mm} \cdot (45,75\text{mm})^2}{1,43\text{mm} \cdot 145,75\text{mm} + 1,43\text{mm} \cdot 45,75\text{mm}}$$

$$z_{eq} = 121,83\text{mm}$$

$$k_{eq} = \frac{\sum_r k_{eff,r} h_r}{z_{eq}} = \frac{1,43\text{mm} \cdot 145,75\text{mm}1,43\text{mm} \cdot 45,75\text{mm}}{121,83\text{mm}}$$

$$k_{eq} = 2,25\text{mm}$$

The initial rotational stiffness can then be determined for $\mu = 1$:

$$S_j = \frac{Ez^2}{\mu \sum \frac{1}{k_i}} = \frac{210000\text{MPa} \cdot (95,75\text{mm})^2}{1 \cdot \left(\frac{1}{k_1} + \frac{1}{k_2} + \frac{1}{k_{eq}} \right)}$$

$$S_j = 3052,70\text{kNm}$$

C. Newton-Raphson

In this appendix the Newton-Raphson method for establishing the behaviour of a non-linear model. This appendix is based on Cook et al., 2002.

Linear models tend to provide results which are suitable approximations for common and everyday problems which involves engineering. However, non-linearity is a common problem as materials in the perspective of structural mechanics often behave non-linearly. Non-linearity of a material could be non-linear elasticity, plasticity and creep and is non-linear due to the stiffness of the material becomes a function of the displacement and deformation.

Newton-Raphson is a method to determine the displacement u to the corresponding load P when the material behave non-linear. Considering the initial state where $u = 0$, a load P_1 is then applied and the corresponding displacement u_1 is unknown. The displacement is determined by first estimating the initial tangent stiffness k_{tO}, see figure C.1.

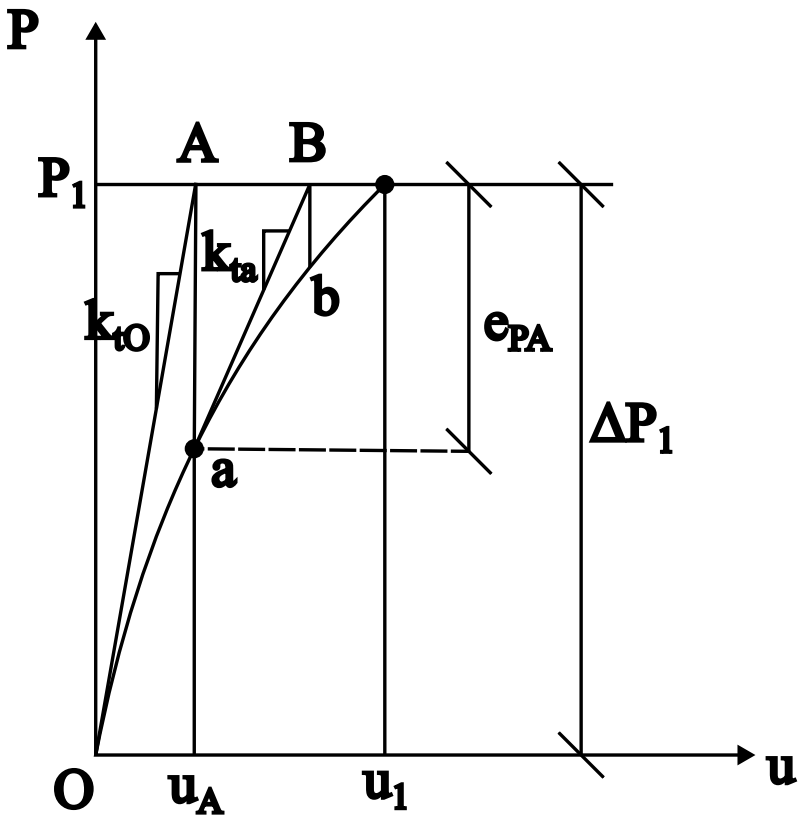

Figure C.1: Iterations to converge at load P_1.

The initial load increment is the load itself, as there is no load at the start. The estimated initial stiffness k_{tO} is used to calculate the current displacement increment.

$$k_{tO}\Delta u = \Delta P_1 \qquad \Delta u = k_{tO}^{-1}\Delta P \qquad u_A = 0 + \Delta u$$

u_a is the current estimate of the of u_1 and are not exact due to the deformation not corresponding to the load P_1. The load imbalance e_{PA} can then be determined as:

$$e_{PA} = P_1 - ku_A$$

k is the stiffness evaluated at displacement u_A and ku_A would then equal the load P_a. The idea is then to reduce the load imbalance to zero by iterations. The load P_1 is kept constant and another step is taken from point a with the tangent of k_{ta}. This results gives a displacement of u_B which is a more accurate displacement for the load P_1. The load increment from point a is e_{PA} and the current displacement increment is determined and updated:

$$k_{ta}\Delta u = e_{PA} \qquad \Delta u = k_{ta}^{-1} e_{PA} \qquad u_B = u_A + \Delta u$$

The force at displacement u_B is still not equal to P_1 and the current load imbalance is then:

$$e_{PB} = P_1 - ku_B$$

k is the stiffness evaluated at displacement u_B and ku_B would then equal to the load P_b. The next step is to move along another tangent beginning at point b. This iterations step is repeated and the next iteration would come closer to a deflection which corresponds to the load P_1. The more iterations that are performed, the closer the load imbalance gets to zero and the displacement will tend to u_1. The next load increment P_2 can then be added and the iterations are repeated until the corresponding displacement u_2 are reached.

D. Slope-deflection method

The method of determining the moment distribution at the supports and joints are expanded here. This appendix is based on [Henderson, 2022].

The slope-deflection method is used to determine the bending moments at the frame supports and the joints. The slope-deflection method establishes a relation between the end moments and the rotation as well as the displacement of the considered element. Equations are developed that describes the relations when considering the curvature of the element. The slope-deflection method can be used to analyse statically determinate and indeterminate beams and frames.

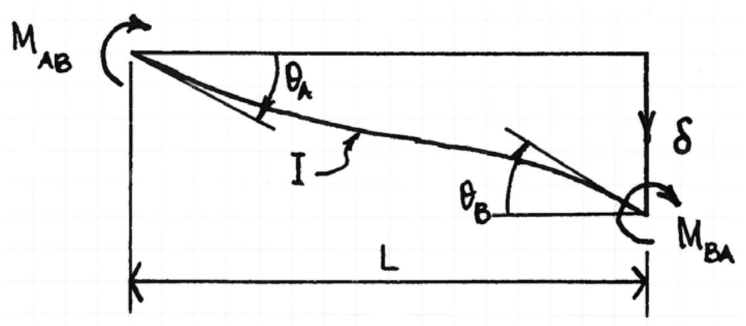

Figure D.1: Illustration of the support conditions of the beam.

Considering the beam element shown in figure D.1, the equations are given as:

$$M_{AB} = \frac{2EI}{L}\left(2\theta_A + \theta_B - \frac{3\delta}{L}\right) - M_F \tag{D.1}$$

$$M_{BA} = \frac{2EI}{L}\left(\theta_A + 2\theta_B - \frac{3\delta}{L}\right) - M_F \tag{D.2}$$

Where

M_{AB}, M_{BA}	is bending moment at A and B respectively
θ_A, θ_B	is the rotation at A and B respectively
δ	is the relative deflection
M_F	is the fixed-end moment

The frame can be divided into three individual elements: two columns connected to the beam, see figure D.2. Point C is used to indicate the middle of the beam. The sum of the moment at a joint is equal to zero. So at B where element A-B and B-D connects, the moments $M_{BA} + M_{BC} = 0$. The frame is symmetrical and the members are assumed axially rigid which results in the relative displacement $\delta = 0$.

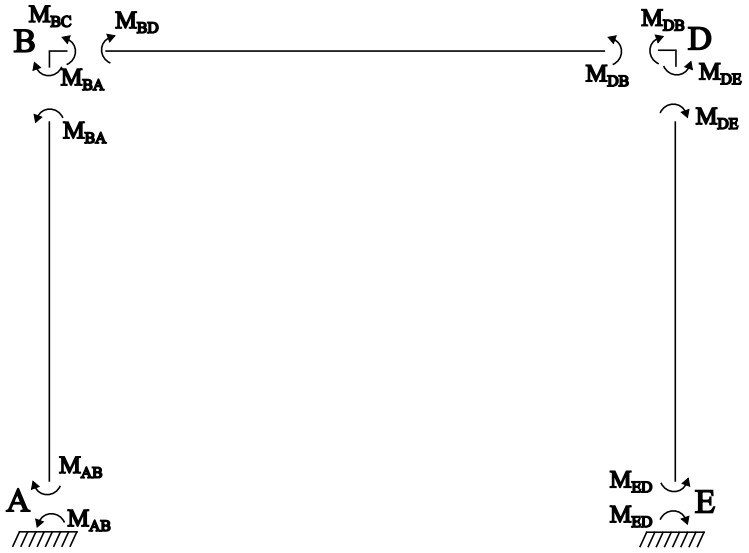

Figure D.2: Illustration of the elements and internal moments of the frame.

Considering a single element AB with a rotation at each end, see figure D.3, the end-moments can be described in equation (D.3).

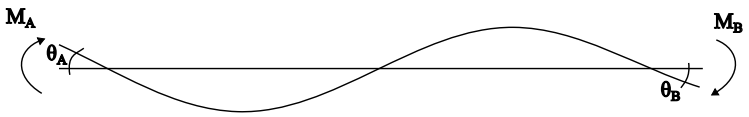

Figure D.3: Illustration of the beam with end moments and rotation.

$$M_A = \frac{4EI}{L}\theta_A + \frac{2EI}{L}\theta_B \tag{D.3}$$

For a beam with fixed connection with a uniform load q, see figure D.4, the fixed-end moments are given in equation (D.4).

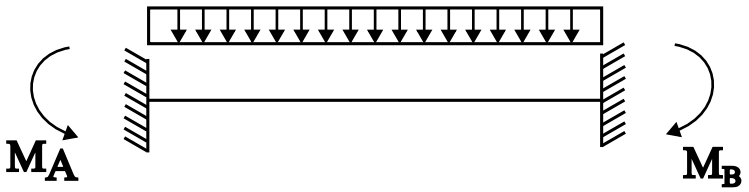

Figure D.4: The moments of a fixed beam with a line load q.

$$M_A = -\frac{qL^2}{12} \tag{D.4}$$

From figure D.3 the rotation at A and B are equal but in the opposite direction. Using the principle of superposition the moment at A is determined in equation (D.5).

$$M_A = \frac{2EI}{L}\theta - \frac{qL^2}{12} \tag{D.5}$$

When introducing a rotational stiffness at the supports and joints the bending moments due to the springs can be denoted $S\theta$, where S is the rotational spring and θ is the rotational spring. The sum of the bending moment in the column and bending moment due to the spring is equal to 0, this is expressed in equation (D.6).

$$S_A\theta_A + \frac{2EI_c}{H}(2\theta_A + \theta_B) = 0 \tag{D.6}$$

Likewise the slope-deflection equations can be used at the joints, see equation (D.7).

$$\frac{M_{BD}L}{2EI_b} + \frac{M_{BD}}{S_B} = 2\theta_B + \theta_D \tag{D.7}$$

Solving for the bending moments at the support and the joints then give the Kleinlogel-type formulations, see equation (D.8) and equation (D.9).

$$M_A = \frac{qL^2}{12}\frac{(1-2K_A)K_B}{(2-K_A+kK_B)} \tag{D.8}$$

$$M_B = -\frac{qL^2}{12}\frac{(2-K_A)K_B}{(2-K_A+kK_B)} \tag{D.9}$$

K_A and K_B are coefficients which are dependent on the stiffness of the column feet and joint respectively. They are determined from equation (D.10).

$$K_A = \frac{2EI_c}{S_{jA}H + 4EI_c};\ K_B = \frac{S_{jB}H}{S_{jB}H + 4EI_c} \tag{D.10}$$

Where:

k	is equal to $\frac{I_bH}{I_cL}$
S_{jA}	is the rotational stiffness of the support
S_{jB}	is the the rotational stiffness of the joint
H	is the height of the frame
L	is the length of the frame

E. Bending moment at the centre of a beam

The bending moment at the centre of the beam is derived, when the end-moments are known, in this appendix.

The internal bending moment at the centre of the beam is determined with the use of equilibrium analysis. Figure E.1 shows the forces acting on the beam. The supports are shown as pinned with a rotational stiffness.

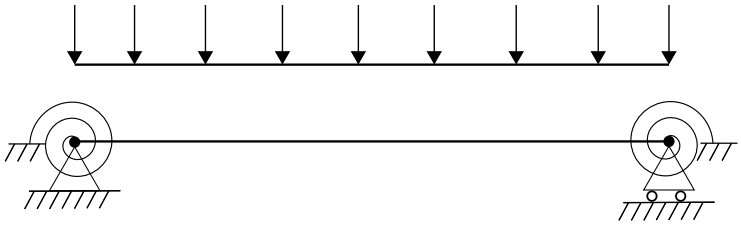

Figure E.1: Illustration of the support conditions of the beam.

The free body diagram of the beam can be seen in figure E.2. Due to the rotational stiffness, a moment is developed at the supports. The forces at each supports are identical due to the frame being symmetrical at centre of the beam. The bending moments M_0 are known from the slope-deflection method and V_0 is given as half the distributed load summarised over the beam length.

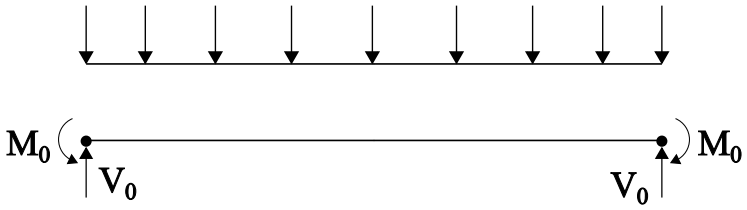

Figure E.2: Free body diagram of the beam.

To determine the internal bending moments, the beam is divided such the sections forces are illustrated in figure E.3.

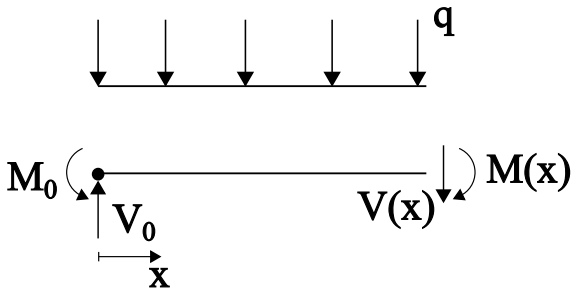

Figure E.3: Section forces of the beam.

Determining the moment at the cut of the beam gives the equation:

$$M(x) - M_0 + qx - \frac{qx^2}{2} = 0 \tag{E.1}$$

$$\Downarrow$$

$$M(x) = M_0 - qx + \frac{qx^2}{2} \tag{E.2}$$

The bending moment at Point C where $x = L/2$ is determined from equation (E.3).

$$M(L/2) = M_0 - \frac{qL}{2} + \frac{q(L/2)^2}{2} \tag{E.3}$$

This is the bending moment at the centre of the beam with supports with a rotational stiffness.